Spin–orbit-induced photoelectron spin polarization in angle-resolved photoemission from both atomic and condensed matter targets

2012 J. Phys.: Condens. Matter 24 173001

(http://iopscience.iop.org/0953-8984/24/17/173001)

IOP PUBLISHING JOURNAL OF PHYSICS: CONDENSED MATTER

J. Phys.: Condens. Matter **24** (2012) 173001 (30pp) doi:10.1088/0953-8984/24/17/173001

TOPICAL REVIEW

Spin–orbit-induced photoelectron spin polarization in angle-resolved photoemission from both atomic and condensed matter targets

Ulrich Heinzmann[1] **and J Hugo Dil**[2,3]

[1] Faculty of Physics, University of Bielefeld, Universitätsstrasse, D-33501 Bielefeld, Germany
[2] Physik-Institut, Universität Zürich, Winterthurerstrasse 190, CH-8057 Zürich, Switzerland
[3] Swiss Light Source, Paul Scherrer Institute, CH-5232 Villigen PSI, Switzerland

E-mail: uheinzm@physik.uni-bielefeld.de and jan-hugo.dil@psi.ch

Received 29 November 2011, in final form 26 January 2012
Published 5 April 2012
Online at stacks.iop.org/JPhysCM/24/173001

Abstract

The existence of highly spin polarized photoelectrons emitted from non-magnetic solids as well as from unpolarized atoms and molecules has been found to be very common in many studies over the past 40 years. This so-called Fano effect is based upon the influence of the spin–orbit interaction in the photoionization or the photoemission process. In a non-angle-resolved photoemission experiment, circularly polarized radiation has to be used to create spin polarized photoelectrons, while in angle-resolved photoemission even unpolarized or linearly polarized radiation is sufficient to get a high spin polarization. In past years the Rashba effect has become very important in the angle-resolved photoemission of solid surfaces, also with an observed high photoelectron spin polarization.

It is the purpose of the present topical review to cross-compare the spin polarization experimentally found in angle-resolved photoelectron emission spectroscopy of condensed matter with that of free atoms, to compare it with the Rashba effect and topological insulators to describe the influence and the importance of the spin–orbit interaction and to show and disentangle the matrix element and phase shift effects therein.

The relationship between the energy dispersion of these phase shifts and the emission delay of photoelectron emission in attosecond-resolved photoemission is also discussed. Furthermore the influence of chiral structures of the photo-effect target on the spin polarization, the interferences of different spin components in coherent superpositions in photoemission and a cross-comparison of spin polarization in photoemission from non-magnetic solids with XMCD on magnetic materials are presented; these are all based upon the influence of the spin–orbit interaction in angle-resolved photoemission.

(Some figures may appear in colour only in the online journal)

Contents

1. Introduction

Until the publication of the famous paper by Ugo Fano [1] on the theoretical prediction of spin polarized photoelectrons ejected from cesium atoms by means of circularly polarized light, it was believed that the spin polarization of photoelectrons is a relativistic effect, which is only important at high photon energies or high photoelectron velocities ($v/c \sim 1$) or when the charge of the nucleus is large ($Z \sim 100$). Meanwhile we know from many experiments and theoretical calculations that nearly all photoelectrons are highly spin polarized, regardless of whether they are produced by circularly polarized light at free atoms, free molecules, non-magnetic solid and adsorbates or by linearly polarized or even by unpolarized radiation in an angle-resolved photoemission experiment [2]. Spin polarized photoemission on non-magnetic systems, known for decades as the 'Fano effect' [3], has experienced a renaissance over recent years, whilst strong interest has also grown in an aspect of surface physics known as the 'Rashba effect' [4], a complete spin splitting of momentum-resolved surface states. These effects are all based jointly on the influence of the spin–orbit interaction.

In 1970 Ugo Fano [5] named the reason for the existence of spin polarized photoelectrons as 'spin–orbit coupling: a weak force with conspicuous effects'. Although the spin–orbit interaction is weak and its fine structure splitting is small, the spin polarization of photoelectrons is often complete, i.e. 100%.

It is the goal of the present paper to cross-compare selected experimental results of spin-resolved photoelectron spectroscopy in the gas phase of free atoms with spin- and angle-resolved photoemission of condensed matter and to explain the joint basic influence of the spin–orbit interaction. There are some topical reviews in the literature [2, 3, 6–12] which cover partial aspects of spin polarized photoemission due to spin–orbit interaction.

The only precondition for getting spin polarized photoelectrons from non-magnetic systems is that the influence of the spin–orbit interaction is resolved somewhere in the experiment, spectroscopically, by use of monochromatic radiation to resolve the fine structure splitting of the initial or the final state, or by use of an electron spectrometer to resolve the fine structure splitting of the final state (ionic state or hole state), or by studying emission angle-resolved. The first experimental verification of the Fano effect was performed as predicted with free cesium atoms: figure 1 shows the experimental results [13, 14] in cross-comparison with Ugo Fano's prediction [1]. A pronounced spin polarization of photoelectrons angle integrated extracted by an electric field was measured along the direction of the helicity of the radiation to be between +100% and −50%, the positive and negative sign indicating parallel and antiparallel spin polarization direction relative to the light helicity, respectively.

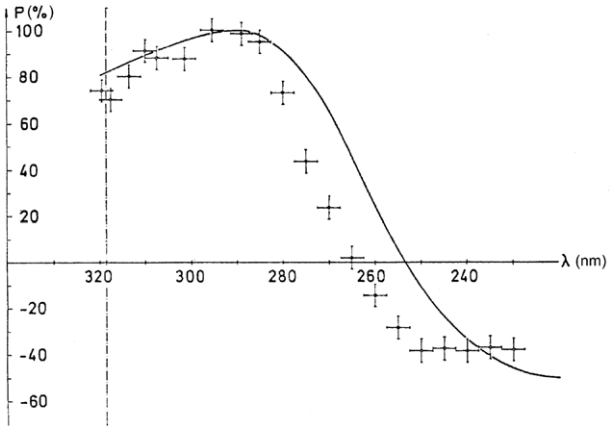

Figure 1. Emission angle integrated spin polarization of photoelectrons ejected by circularly polarized uv light from cesium atoms and extracted by means of an electric field. Experimental error bars [13, 14] and theoretical prediction (curve [1]) (the Fano effect). Positive spin polarization means parallel to the light helicity; at the photon wavelength of 290 nm all photoelectrons produced regardless of their direction of emission have a complete spin polarization parallel to the photon spin. From [13].

Since the photoelectrons are ejected from the $6s_{1/2}$ ground state no spin–orbit interaction is present in this initial state. The spin–orbit interaction shows its effect here in the difference of matrix elements for transitions into the p continuum states. $R_{1/2}$ and $R_{3/2}$, the radial dipole matrix elements for transitions into the non-equal continua $p_{1/2}$ and $p_{3/2}$, are different due to the influence of the spin–orbit interaction as shown in figure 2: the two radial matrix elements vanish at different photon energies creating a spin–orbit splitting of the position of the deep minimum of the photoionization cross section (so-called Cooper minimum) given by the square of the corresponding dipole matrix element [1]. When $R_{3/2} = -2R_{1/2}$ [14] the spin polarization of all photoelectrons, regardless of their direction of emission, is 100% parallel to the photon spin. This effect is a complete spin polarization transfer from the photons onto the photoelectrons due to a matrix element effect for transitions where spin and orbit are parallel ($p_{3/2}$) or antiparallel ($p_{1/2}$). Further on, similar matrix element effects also occur in spin-resolved photoemission in condensed matter: the experimental photoemission results of alkali layers [15, 16]

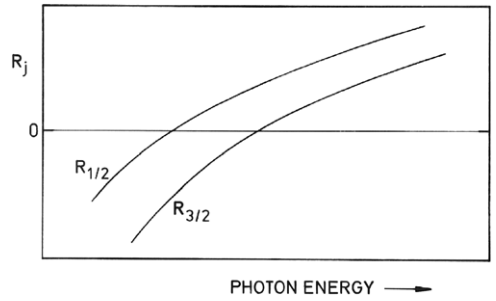

Figure 2. The radial matrix elements $R_{1/2}$ and $R_{3/2}$ for optical transitions from the $s_{1/2}$ ground state to the spin–orbit-induced different continua $p_{1/2}$ and $p_{3/2}$, respectively, have different zero crossings as a function of the photon energy. These zero crossings define a Cooper minimum of the cross section [1].

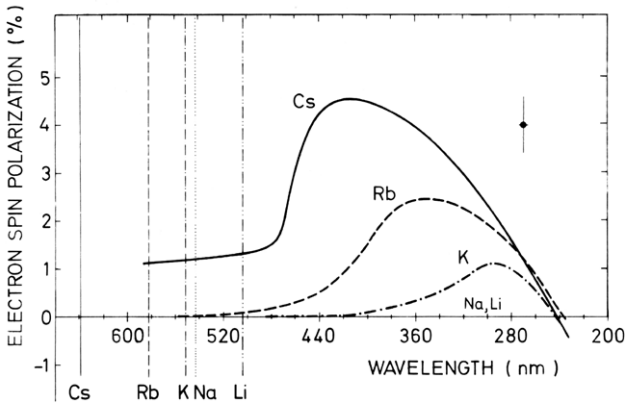

Figure 3. Comparison of the emission angle integrated photoelectron spin polarization ejected by circularly polarized light from different solid alkali films. The curves denote the averaged experimental results. Their statistical uncertainties are described by the size of the single error bar shown outside the curves [15, 16]. Adapted from [15, 16].

and of a GaAs crystal [17] are given in figures 3 and 4, respectively. In GaAs the transition is reversed to the above-discussed case of cesium atoms: the initial states are the spin–orbit interaction fine structure split $p_{1/2}$ and $p_{3/2}$ states and the final band is $s_{1/2}$: however, also here the different matrix elements define the spin polarization values of the photoelectrons (see figure 5).

Figure 6 shows the set-up of a typical UHV apparatus for the measurement of an angle- and spin-resolved photoemission experiment [18]. Elliptically polarized radiation with a large amount of circular polarization (more than 90%) either from a helical undulator [19] or emitted out-of-plane (above or below) of a synchrotron [20] or from a discharge lamp and use of a linear polarizer and a quarter-wave plate [21] or from a laser [22] (to resolve the rotational states of a molecule) hits the target, mostly in normal incidence.

The photoelectrons emitted normally (as shown in figure 6) or at any emission angle are analyzed with respect to their spin polarization by means of Mott scattering at energies after acceleration between 30 and 100 keV [3, 23, 24]. The spin polarization is given by the left/right or up/down scattering asymmetry. Solid crystal surfaces are prepared and analyzed by means of typical surface physics techniques as shown in figure 6.

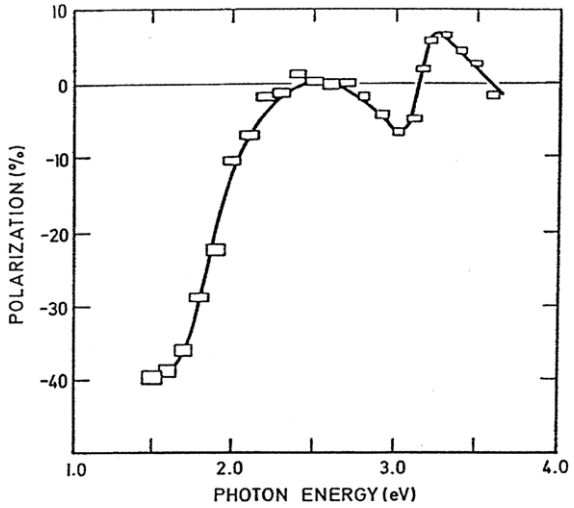

Figure 4. Spin polarization of photoelectrons parallel to the light helicity emitted from cesiated GaAs(110) single crystal by means of circularly polarized light. Reproduced with permission from [17]. Copyright 1976 American Physical Society.

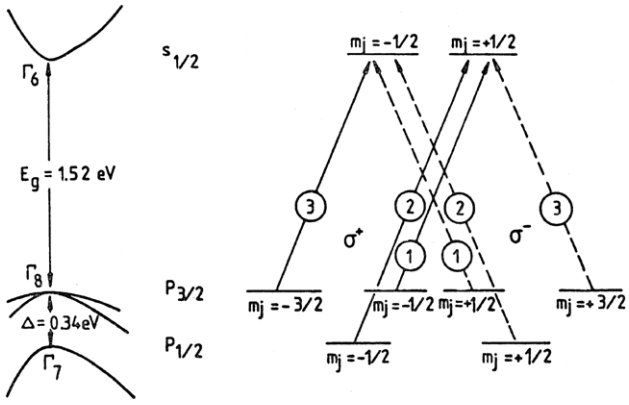

Figure 5. On the left: energy bands of GaAs near the Γ-point with the spin–orbit fine structure splitting of the valence bands. On the right: the degenerate states at $k = 0$ are labeled by their m_j quantum numbers. The allowed transitions for $\sigma^+(\Delta m_j = +1)$ and $\sigma^-(\Delta m_j = -1)$ circularly polarized light are shown as solid and dashed arrows, respectively. The circled numbers represent the relative transition probabilities. Reproduced with permission from [17]. Copyright 1976 American Physical Society.

In the following section 2, the spin polarization transfer due to matrix elements effects in experiments using circularly polarized radiation is further discussed in photoionization and photoemission. In sections 3 and 4 the focus moves to the influence and importance of phase shift effects on photoelectron spin polarization when even unpolarized or linearly polarized radiation is used. Here the photoelectron emission from atoms as well as from solids has to be studied emission angle-resolved. In section 5 the relationship of the energy dispersion of these phase shifts obtained in spin-resolved photoelectron spectroscopy with the time delay of photoelectrons emitted as recently measured in attosecond-resolved photoemission is discussed.

In section 6 influences of chiral target structures in addition to the spin–orbit interaction on the photoelectron spin polarization are presented. In section 7 recent results

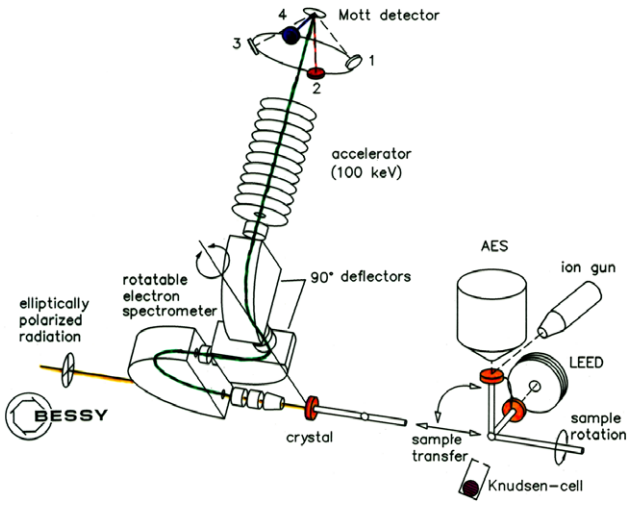

Figure 6. Experimental set-up of the apparatus for angle and spin polarization resolved photoemission spectroscopy at solid surfaces used at the electron storage ring BESSY in Berlin [18] and in further experiments. Low energy electron diffraction (LEED) and Auger electron spectroscopy (AES) is used to characterize the order and cleanness of the crystal surface in the preparation chamber, respectively. Adapted from [18].

of the Rashba effect and topological insulators are presented and discussed. In section 8 the spin–orbit-induced coherent superposition of spins is reviewed and in section 9 the cross-comparison of spin polarized photoemission from magnetic materials measured in the paramagnetic phase (above the Curie temperature) with XMCD of the same material (below the Curie temperature) is presented in order to show up how spin–orbit interaction is present and should be taken into account, even for magnetic materials where exchange interaction is dominant and additionally influences the spin orientation of the photoelectrons. In conclusion section 10 summarizes the influence of the spin–orbit interaction in spin- and angle-resolved photoemission experiments. It should be noted that this paper does not review the important theoretical work performed in spin-resolved photoemission which would be, of course, a second review article of similar length. Important aspects are discussed in [7, 25–27].

2. The spin polarization transfer from spin (circularly) polarized radiation onto the photoelectrons: the matrix element effect in photoelectron spin polarization

Already in figure 1 an example is presented for uv light of 290 nm, where all photoelectrons ejected from cesium atoms by means of circularly polarized light are completely spin polarized regardless of their direction of emission. This measured case exists where the radial matrix elements for the $s \rightarrow p_{3/2}$ and $s \rightarrow p_{1/2}$ optical transitions relate to each other by a factor of -2. Here the photoelectron spin polarization always coincides in its direction with the photon spin for left or for right circular light polarization. Thus this effect can be seen as a complete spin polarization transfer from the photons to the photoelectrons. In the presence of spin–orbit interaction orbital angular momentum quantum

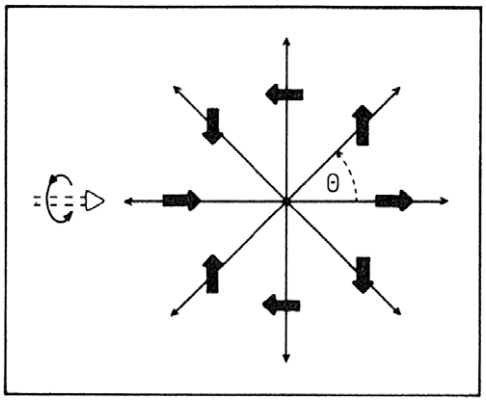

Figure 7. A rotating spin polarization vector of complete polarization at all emission angles θ in the reaction plane defined by the photon and the photoelectron momenta. σ^+ circularly polarized light is incident from the left. There are the two spin polarization components (projections of the spin polarization vector shown) of the photoelectrons ejected from thallium atoms at a radiation wavelength of 83 nm [28]. The spin polarization component perpendicular to the plane shown is zero for all θ. From [28].

numbers m_l are no longer 'good' quantum numbers. Thus the optical transitions no longer follow the selection rules $\Delta m_l = \pm 1$ (an increase of the orbital angular momentum for the use of circularly polarized light). The transitions follow the selection rules $\Delta m_j = \pm 1$ with the consequence that a spin polarization may arise in the final state, in some cases as discussed above even a complete one. A similar effect of a complete spin polarization transfer to the photoelectrons has been measured with free thallium atoms, where again all photoelectrons produced are completely spin polarized; however, the polarization vector rotates in the photoemission plane when the photoelectron emission is studied angle-resolved. Figure 7 shows the experimental result [28] of the spin polarization vector (amount to be 1, i.e. a 100% spin polarization) in the plane defined by the photon momentum and the photoelectron momentum. The arrows show the directions of the spin polarization vector; they all reverse their direction by 180° if the light helicity is switched from right-handed to left-handed.

This special case happens with thallium atoms at a photon wavelength of 83 nm. The measured values [28] of the spin polarization component $P(\theta)$ parallel to the photon spin as a function of the emission angle is presented in figure 8 together with a fit according to the equation

$$P(\theta) = \frac{A - \alpha P_2(\cos\theta)}{1 - \beta/2 P_2(\cos\theta)} \qquad (1)$$

where $P_2(\cos\theta) = 3/2\cos^2\theta - 1/2$ is the second Legendre polynomial and A, α and β are the dynamical parameters describing the intensity and spin polarization distributions in angle-resolved photoelectron emission spectroscopy. A is also the angle integrated spin polarization, when all photoelectrons are studied regardless of their direction of emission by use of an electric field as discussed in section 1 and shown in figures 1 and 3, since the angle integration of the second Legendre polynomial is zero in equation (1).

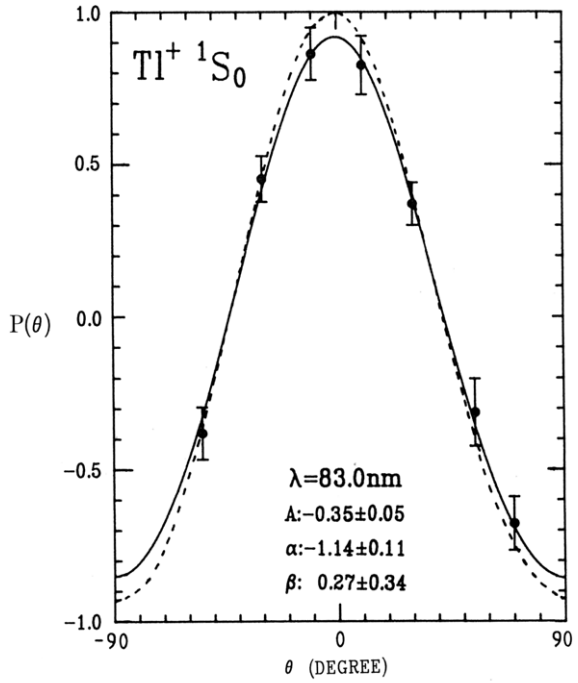

Figure 8. Angular dependence of the spin polarization component $P(\theta)$ parallel to the radiation helicity (see figure 7) at 83 nm photoionization wavelength for thallium atoms. The solid line drawn through the data points represents a least-squares fit yielding the dynamical parameters given in the figure. The dashed curve is the deconvoluted curve for a zero angular acceptance cone of the electron spectrometer used [28]. From [28].

β is the asymmetry parameter of the differential photoemission cross section describing the angular dependence of the photoelectron intensities and α describes the angular dependence of the spin polarization component along the direction of the light helicity. It is worth noting that, for the special case shown in figures 7 and 8, the three dynamical parameters as well as the total photoionization cross section only depend upon two real radial dipole matrix elements $R_{3/2}$ and $R_{1/2}$ describing the optical transitions from p to $d_{3/2}$ and $s_{1/2}$ continuum states. It should further be mentioned that at 83 nm within an autoionizing resonance (or in 'resonant photoemission' in the language of condensed matter) this special case appears with the relation of both radial matrix elements being $R_{3/2} = 2R_{1/2}$ [28], very similar to the case of the Fano effect with free cesium atoms (see section 1) and also yielding a complete spin polarization vector of all photoelectrons in the photoemission plane. Again the spin polarization of photoelectrons only depends upon two matrix elements in a special ratio to each other to create a complete spin polarization transfer in photoemission with circularly polarized radiation.

There are two possible cases to obtain a complete spin polarization of electrons in final states after a photoabsorption process. Either the final state is a quantum mechanical pure state, i.e. it consists only of one magnetic substate, for example fulfilled in $p_{1/2} \rightarrow s_{1/2}$ transitions with σ^+ light as shown in figure 5 right part. It is worth noting in this section that in this case, for a reason discussed later, no transition to a d final state may occur. In the other case, the complete spin polarization occurs if all final states of different spin polarization are coherently superposed and interfere with each other in photoemission and the 'wrong' spin part is destructively suppressed in interference.

This second case is fulfilled in the two examples discussed so far, the photoionization in cesium and thallium atoms with the relationship of $R_{3/2} = \pm 2R_{1/2}$ for the two radial dipole matrix elements defining the amplitudes of two interfering wavefunctions describing the photoelectron final states. It is worth noting that a quantum mechanical interference can only occur in the final states if they have the same energy and if they are reached in optical transitions from the same single initial state according to (different) selection rules.

The first case, where only one final magnetic substate is occupied, is the common one in condensed matter physics, where the photoemission process is angle-resolved studied in certain emission geometries of high crystal symmetry. For example, if the photoemission of a (100) surface of a cubic crystal is studied in normal incidence and at an electron emission angle normal to the surface the spherical harmonic Y_{lm_l} describing the angular distributions of photoelectron intensity as well as of spin polarization vanishes at the emission angle $\theta = 0$ for $m_l \neq 0$. Thus for $\theta = 0$ all existing final states have $m_j = m_s = \pm 1/2$ ($m_l = 0$) [26] with a spin polarization completely parallel or antiparallel to the light helicity. This is demonstrated in figure 9 for normal incidence and normal photoemission of a krypton monolayer adsorbed on a Pt(111) surface [29]. In the right part of figure 9 the allowed transitions are shown starting from p bands. Since the energy degeneracy is lifted for $p_{3/2}$ $m_j = \frac{3}{2}$ and $\frac{1}{2}$ bands (due to the crystal field splitting) all final states occupied are—quite unlike the free-atom case also shown—pure spin states $-\frac{1}{2}$ for transition 1 and $+\frac{1}{2}$ for transitions 2 and 3 if σ^+ circularly polarized radiation is used ($\Delta m_j = +1$). In the left part of figure 9 upper part the experimental results [29, 9] of the photoelectron spin polarization show that there are three peaks in the photoelectron spectrum of complete spin polarization $+1$ or -1 describing the symmetry (i.e. the quantum numbers) of the initial states the electrons come from. Note that in the middle part of the left figure in figure 9 the polarization actually measured was not always 100% since all photoemission peaks have certain widths and partially overlap in energy and show inelastic scattering wings which can be deconvoluted by combination of the spin polarization (middle part) and the total intensity (lower part) values.

Spin polarization measurements with circularly polarized radiation in a photoemission direction normal to the crystal surface can be used for a symmetry resolved band mapping according to the positive or negative (complete) spin polarization values measured. This is shown in figures 10 and 11 for photoemission with Ir(111) [30] with four peaks in the photoemission spectrum of the conduction band some electronvolts below the Fermi energy E_F: A, B, C and D with positive, negative, negative and positive spin polarization, respectively. They correspond to the transitions drawn in the band structure [31, 32] in figure 11 mapping the $\Lambda_{4^+ +5^+}$ and

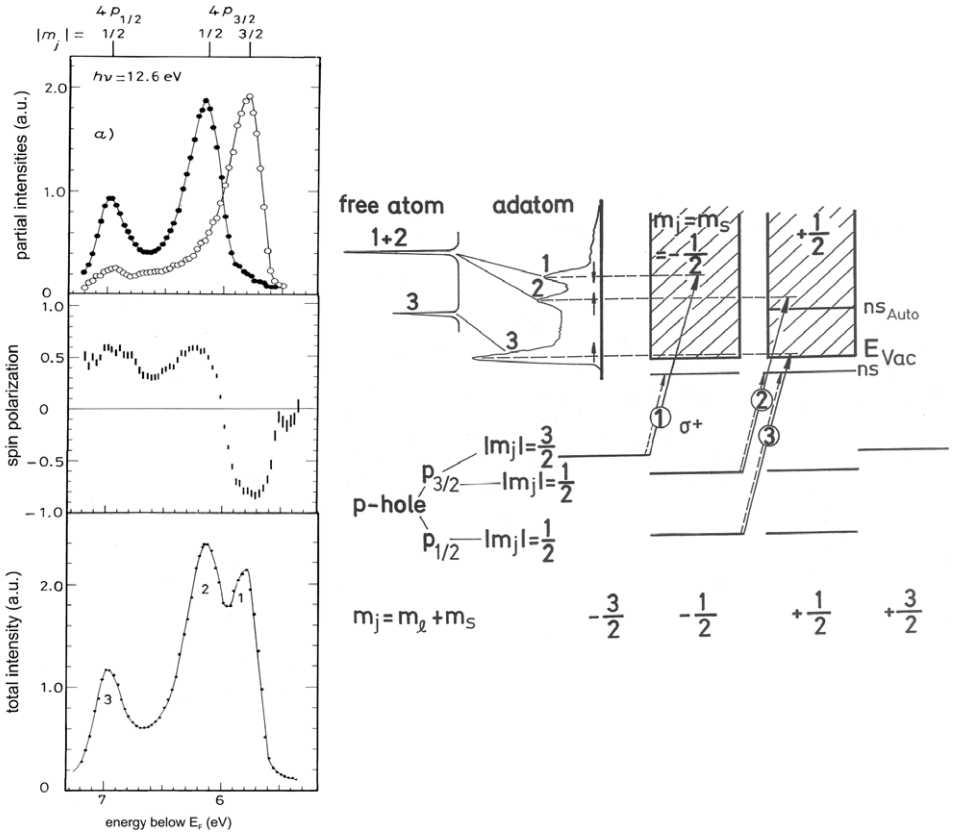

Figure 9. Right part: schematic diagram of the transitions in rare gas adsorbates by use of σ^+ circularly polarized radiation taking into account the selection rule ($\Delta m_j = 1$). Contrary to the case of free atoms the $p_{3/2}$ hole magnetic substates are no longer energy degenerate due to crystal field splitting, with the consequence that all peaks in the photoelectron spectrum correspond to final pure spin states with $m_s = -1/2$ or $1/2$. This is valid for normal photoemission. Left part: spin polarized photoemission of a krypton monolayer on Pt(111) at a photon energy of 12.6 eV in normal photoelectron emission and normal photon incidence. Experimental results [29] of the total (spin-independent) intensity (lower part), electron spin polarization (middle part), and partial intensities for spin parallel (full) and spin antiparallel (open) to the radiation helicity (upper part) (figure adapted from [9]).

Λ_{6^+} bands which in turn correspond to negative and positive spin polarization, respectively.

For the cases discussed in this section the spin polarization measured parallel or antiparallel to the helicity of the radiation used in photoemission is always proportional to the degree of the circular polarization (third Stokes parameter I_3) [21, 33]. In the case $I_3 = 0$, i.e. the radiation is linearly polarized or even unpolarized, photoelectrons emitted normally to the surface should not be polarized. In some cases, however, where anisotropies exist in the phototarget, the angle $\theta = 0$ in the spherical harmonics may differ from the direction of the normal to the surface, with the consequence that interferences of wavefunctions in the final states create spin polarization components which also exist when linearly polarized or even unpolarized radiation is used in angle-resolved photoemission. This will be discussed in the following sections.

3. Phase shift effects in angle- and spin-resolved photoemission: a cross-comparison between atoms and solid adsorbates

When circularly polarized radiation is used and the photoelectron emission process is studied angle-resolved, the photoelectrons are highly spin polarized with a polarization vector consisting of three components with respect to the reaction plane as shown in figure 12. This demonstrates for the dipole approximation, valid in general up to photon energies of 1 keV [26], that it makes no difference whether the left-handed (σ^+) light comes from the left side or right-handed (σ^-) light comes from the right side. This dipole approximation is based upon the fact that the photon momentum is negligibly small compared to the photoelectron momentum and thus no forward/backward asymmetry of the photoelectron intensity takes place. This effect is theoretically accompanied by vanishing quadrupole and higher multipole matrix elements. There are a few exceptions of deviation from this dipole approximation even at small photon energies experimentally observed in spin-resolved photoemission at energies where all dipole matrix elements show zero line crossing values [34]. The two spin polarization components in the reaction plane, defined by the momenta of photon and photoelectron as shown in figure 12, switch their sign (and thus their direction by 180°) if the helicity of the radiation is reversed, since these two components are proportional to the degree of circular polarization [21], as already discussed in section 2.

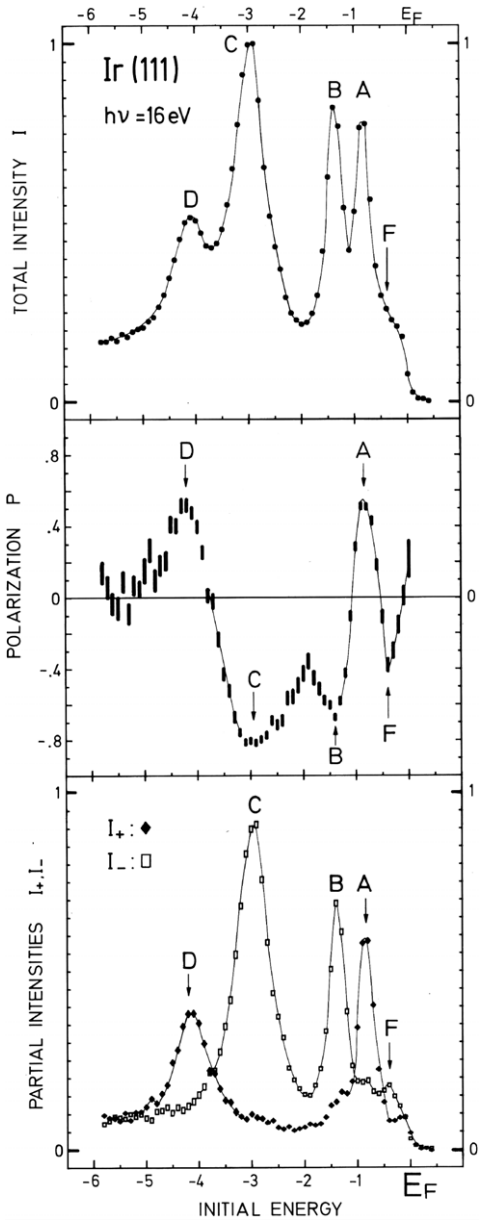

Figure 10. Total intensity I (upper panel), electron spin polarization P (middle panel), and partial intensities I_+ and I_- (lower part) for spin parallel and antiparallel to the helicity of circularly polarized radiation of 16 eV energy, respectively, in normal incidence and normal photoemission at Ir(111) [30]. From [30].

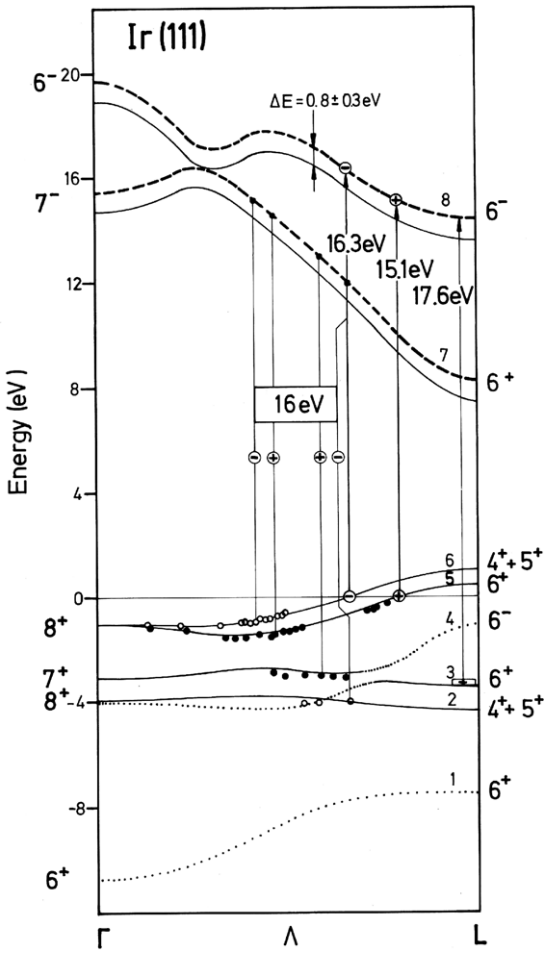

Figure 11. Symmetry-resolved band mapping of Ir(111) by means of spin-resolved photoemission (figure 10). The solid and dotted lines represent a band structure calculation [31]. The signs inserted in the arrows indicate the sign of the spin polarization of photoelectrons measured along normal emission for σ^+ radiation. They follow from relativistic dipole selection rules [32]. The number at the bands characterize their symmetry $\Lambda_{4^+,5^+}$, Λ_{6^+}. Adapted from [30]. The broken lines give the position of the final bands occupied in the photoemission experiment which are shifted to higher energies by $\Delta E = 0.8 \pm 0.3$ eV with respect to the theoretical bands obtained in ground state calculations.

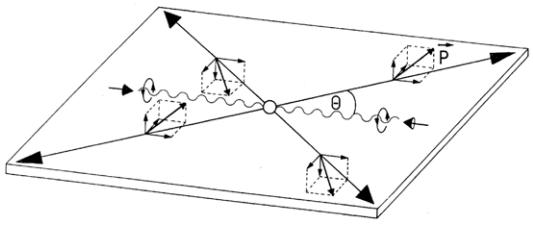

Figure 12. Photoionization reaction plane using circularly polarized radiation with the three components of the spin polarization vector.

This proportionality of the spin polarization with respect to the photon circular polarization is, however, not valid for the third component perpendicular to the reaction plane. For left-handed or right-handed circularly polarized light this component is the same, a helicity reversal does not influence it. Thus an incoherent superposition of right- and left-handed circularly polarized light giving unpolarized radiation or a coherent one giving linearly polarized light should not influence this spin polarization component perpendicular to the reaction plane as shown in figure 13.

This has been experimentally verified in spin- and angle-resolved atomic [35, 36, 2] and molecular [37–39] photoionization in measurements of spin polarized photoelectrons ejected by unpolarized radiation. The spin polarization of photoelectrons perpendicular to the reaction plane by use of unpolarized radiation $P_\perp(\theta)$ is described by [26, 6] by

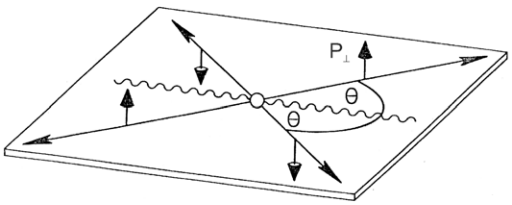

Figure 13. Photoionization reaction plane using unpolarized radiation with a spin polarization of photoelectrons $P_\perp$ perpendicular to the plane.

$$P_\perp(\theta) = \frac{2\xi \sin\theta \cos\theta}{1 - \beta/2 P_2(\cos\theta)} \tag{2}$$

with θ being the emission angle, β and $P_2(\cos\theta)$ being the intensity asymmetry parameter and the second Legendre polynomial as in equation (1), respectively, and ξ being the dynamical parameter describing the order of magnitude of the spin polarization of photoelectrons ejected by unpolarized light. ξ is a parameter not depending upon the angle θ and is a function of the photoelectron energy and is different from atom to atom and from state to state. A similar relationship as in equation (2) is valid for the angular distribution of photoelectron spin polarization if linearly polarized radiation is used [2]:

$$P_\perp(\theta) = \frac{-4\xi \sin\theta \cos\theta}{1 + \beta P_2(\cos\theta)} \tag{3}$$

whereas, however, here the reaction plane is defined by the E vector of the linearly polarized light and the photoelectron momentum. Figure 14 shows for argon atoms the experimental verification of this angular spin polarization as well as intensity dependence (denominator in equation (3)) demonstrating the $\sin\theta\cos\theta$ dependence as being slightly modified by the second Legendre polynomial in the denominator of equation (3) [2, 40].

The existence of the dynamical spin parameter ξ and thus of a non-vanishing spin polarization of photoelectrons perpendicular to the reaction plane $P_\perp$, even if unpolarized radiation is used, is based upon a quantum mechanical interference of two outgoing partial waves describing the photoelectron emission [2]. For example, for photoionization of a rare gas atom with respect to the p shell, leaving behind the ion in a $^2P_{1/2}$ state, ξ reflects this interference by [41]

$$\xi = \frac{3\sqrt{2}}{4} \frac{D_s D_d \sin(\delta_s - \delta_d)}{D_s^2 + D_d^2} \tag{4}$$

with D_s and D_d being the dipole matrix elements for transition from the $p_{1/2}$ orbital to the $s_{1/2}$ and $d_{3/2}$ continuum state, respectively, and $\delta_s - \delta_d$ being the phase shift between the two partial waves reached by means of the selection rules $\Delta j = 1, 0$. There is only a non-vanishing spin polarization if two final channels of different phases exist. Figure 15 shows the values of ξ measured in cross-comparison with theoretical results [36, 41–44, 20] for photoionization of Ar, Kr and Xe atoms in cross-comparison [6]. It is worth noting that the spin polarizations measured and their wavelength dependences given in figure 15 are very similar when comparing Ar, Kr and Xe atoms, apart from the different ionization thresholds. This seems to be surprising on first view, since Ar has a very weak spin–orbit interaction compared to Kr and Xe, as indicated in the fine structure splitting of the ionization thresholds given as vertical dashed lines in figure 15. This demonstrates that the value of the spin–orbit interaction-induced photoelectron spin polarization is not a measure of the strength of the spin–orbit interaction but of the full Coulomb potential with the spin–orbit interaction being only a very small part. On the other hand, without an influence of the spin–orbit interaction no photoelectron spin polarization by use of unpolarized light can be measured, since the ξ values of opposite sign for the fine structure components $^2P_{1/2}$ and $^2P_{3/2}$ as ionic states cancel each other out, as already shown in figure 9: since the photoelectrons from the $4p_{1/2}$ orbital are positively polarized in the continuum state and those from the $4p_{3/2}$ are negatively spin polarized, both peaks in the photoelectron spectrum have to be separated by means of an electron spectrometer in order to measure a photoelectron spin polarization. Also indeed this separation is experimentally more difficult for Ar than for Kr or Xe due to the smaller fine structure splitting. Figure 15 demonstrates that the influence of the spin–orbit interaction has to be resolved somewhere in the experiment by means of an electron spectrometer and by use of monochromatic radiation to separate fine-structure-split (spin–orbit) initial or final states in order to get spin polarized photoelectrons. However, if this is achieved, the spin polarization measured is almost independent of the strength of the spin–orbit interaction [6].

The ξ values measured directly give access to the phase shifts according to equation (4) if the ratio of D_d and D_s is known from the spin polarization results by means of circularly polarized light. Figure 16 gives the measured phase

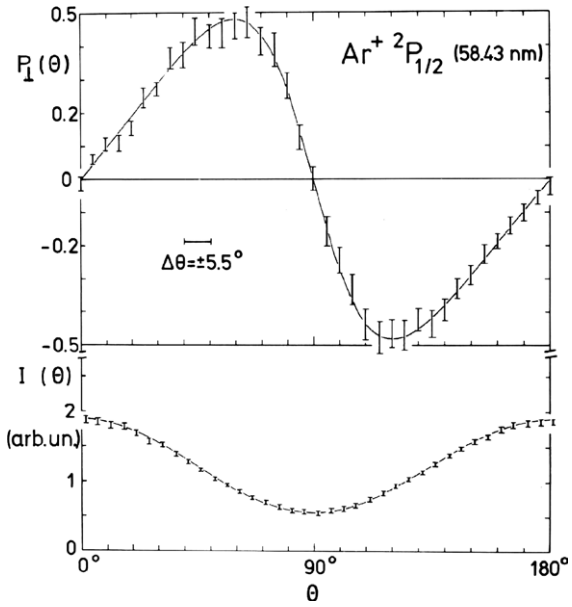

Figure 14. Angular distribution of photoelectron spin polarization (upper curve) and intensity (lower curve) for the photoionization of argon atoms with linearly polarized radiation of 21.22 eV photon energy. The curves are least-squares fits according to equation (3) and its denominator [40, 2]. From [2].

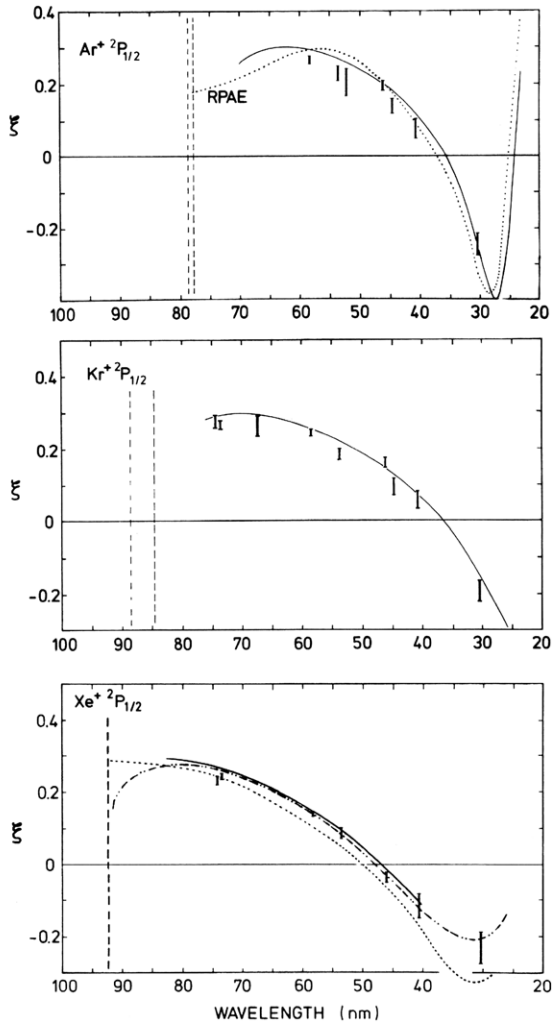

Figure 15. Experimental results (error bars) of the spin parameter ξ for photoelectrons corresponding to the ionic state $^2P_{1/2}$ of Ar (upper panel), Kr (middle panel) and Xe (lower panel) [36, 6] in comparison with theoretical curves: (full) [43], (dashed) [42] and (chain) [44, 41]. The vertical dashed lines represent the spin–orbit split ionization thresholds (the second one of Xe is outside the figure at 103 nm).

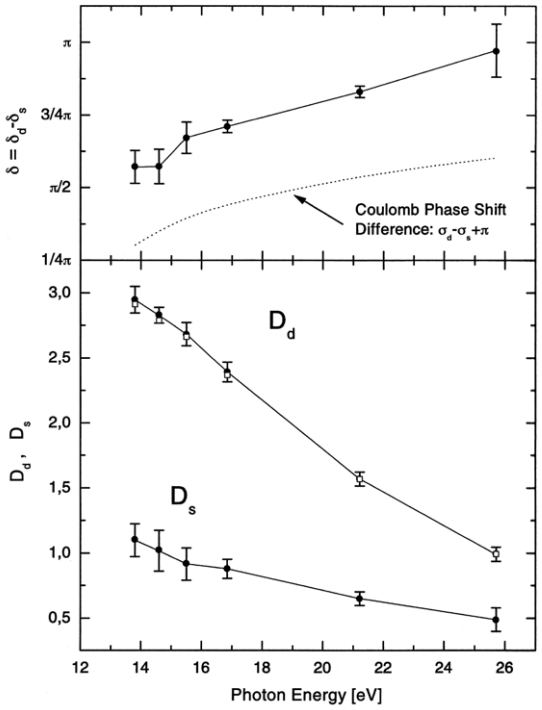

Figure 16. The experimentally obtained dipole matrix elements D_d and D_s with error bars for transitions of $p_{1/2}$ electrons to $d_{3/2}$ and $s_{1/2}$ continua, respectively (lower part), and their corresponding phase shift (upper part) for photoionization of xenon atoms [20, 41, 45]. The solid lines are to guide the eye in comparison with the Coulomb phase shift given as a dashed curve.

shift results together with the corresponding values of D_d and D_s as a function of the photon energy for the photoionization of xenon atoms [20, 41, 45]. The phase shift is the sum of the Coulomb phase shift increasing with the photon energy (the phase shift for photoemission of a hydrogen atom) and of a nearly constant phase shift of about $\pi/4$ which is due to the many-electron effects in xenon which relate to the quantum defects in the discrete photoabsorption spectrum [41].

Figure 17 shows in cross-comparison the angular dependence of the spin polarization component $P(\theta)$ parallel to the light helicity within the reaction plane for atomic photoionization of xenon and the corresponding experimental results for the photoemission from a commensurate xenon monolayer adsorbed on Pd(111) as a function of the emission angle for different photon energies including fitted curves according to equation (1) [46]. It is surprising how accurate the photoemission results in the condensed matter follow the atomic model and the data for gaseous atomic xenon. This is quantitatively supported by the cross-comparison of the spin polarization component perpendicular to the reaction plane $P_\perp$ which is valid also for photoemission with unpolarized radiation for a certain photoelectron emission angle 30° (figure 18) for the xenon adsorbate system and free xenon atoms [46] and shows excellent agreement. Figures 17 and 18 demonstrate that the spin polarization defined as

$$P = \frac{N^+ - N^-}{N^+ + N^-} = \frac{N^+/N^- - 1}{N^+/N^- + 1} \tag{5}$$

only depends upon the intensity ratio for the cases spin parallel and spin antiparallel with respect to a preferential direction. Since the spin–orbit interaction is a local one in the condensed matter and it creates the spin polarization or, in other words, the ratio N^+/N^- different from 1, it is not surprising that the spin-resolved photoemission fulfills the atomic model. Non-spin-dependent intensity effects of a solid given by long range order effects cancel each other out in the ratio N^+/N^-.

Figure 19 additionally shows the angular dependences of the photoelectron as well as the Auger electron spin polarization of a thick rubidium layer condensed on a platinum single crystal. The data can be fitted within the atomic model not only for the primary photoemission process but also for the subsequent Auger decay process emitting spin polarized Auger electrons due to the decay of a spin polarized photohole state [47]. Photoelectron emission of inner core

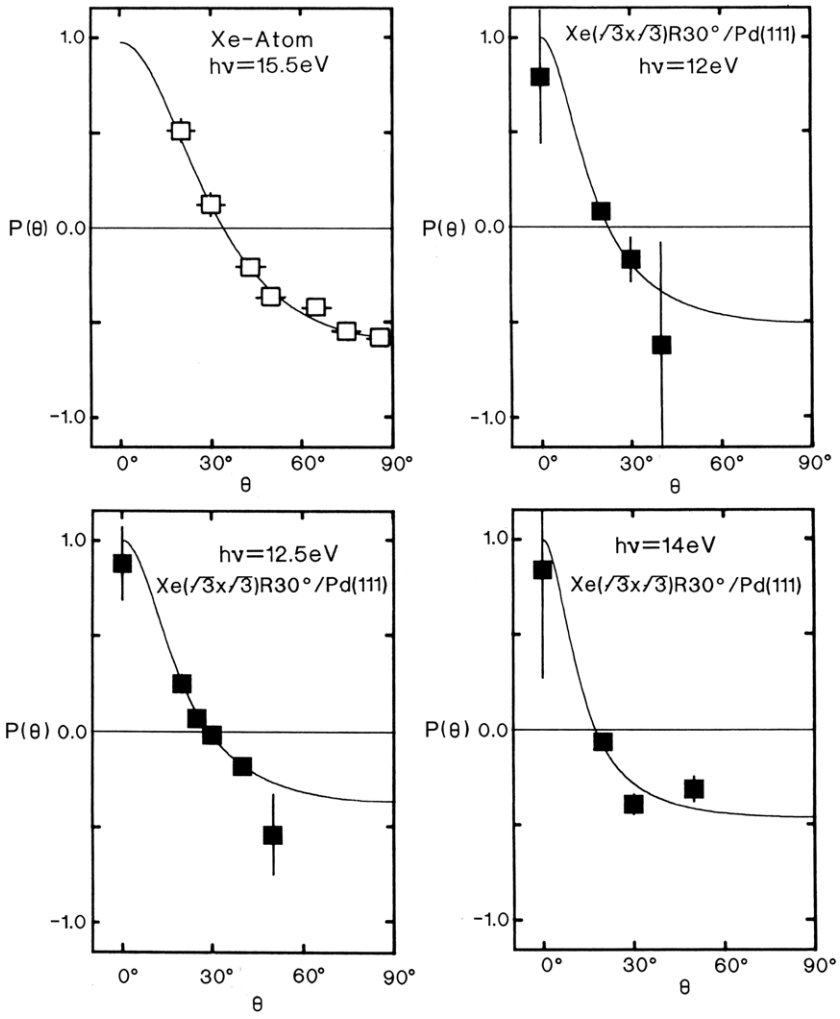

Figure 17. Spin polarization component $P(\theta)$ parallel to the light helicity as a function of the emission angle θ: uppermost left, photoionization of Xe atoms with final ionic state $Xe^{+}\,^{2}P_{1/2}$; other, photoemission from adsorbed $Xe(p_{1/2})$ [$(\sqrt{3} \times \sqrt{3})$ R30° Pd(111)] at different photon energies [46]. Adapted from [46].

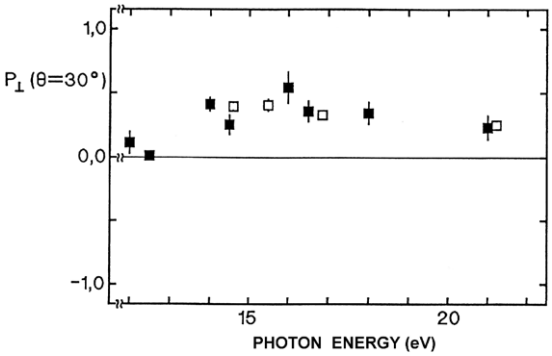

Figure 18. Spin polarization component perpendicular to the reaction plane for photoemission of $Xe(p_{1/2})$ as a function of the photon energy at a polar emission angle of $\theta = 30°$. Closed squares: adsorbate system as in figure 17; open squares: free Xe atoms [46]. From [46].

shells and valence bands create holes which are generally spin-oriented as the emitted photoelectrons. Singlet Auger decays fill up these holes and emit in general Auger electrons with a spin polarization of opposite direction compared to the photoelectron one as shown in figure 19.

4. Phase-shift-determined spin polarization in the angle-resolved photoemission of metal single crystals

The results of measured spin polarization of photoelectrons emitted from free atoms and rare gas adsorbates by unpolarized radiation as discussed in section 3 gave impetus to new efforts to study the photoemission of single crystals in the same way. And indeed we found that the photoelectrons emitted from Pt and Au single crystals by unpolarized radiation are also spin-polarized with a spin polarization vector $P_{\perp}$ perpendicular to the reaction plane, which is for this case defined by the momenta of the photons absorbed and the photoelectrons detected. Figure 20 shows the corresponding experimental set-up: unpolarized photons of a discharge lamp hit the surface of the crystal at an angle of incidence of 62°and the photoelectrons normal to the surface emitted are energy analyzed by means of an electron spectrometer and are accelerated to the Mott detector for the measurement of their

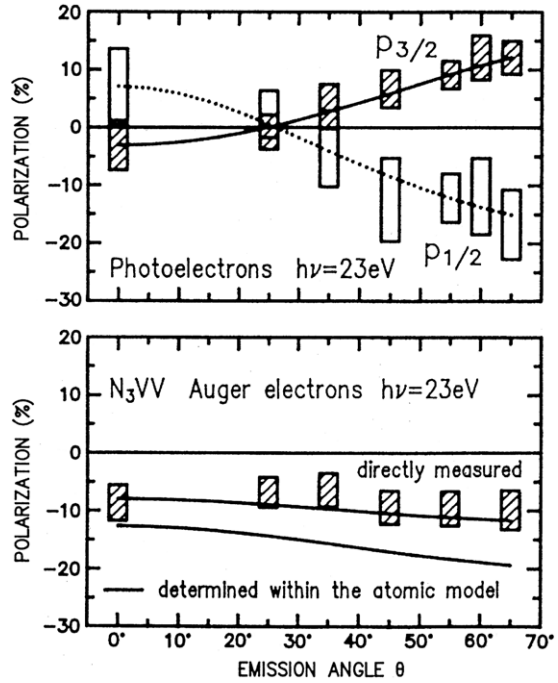

Figure 19. Measured angular dependences of the spin polarization component in the direction of the radiation helicity for photoelectrons as well as for Auger electrons emitted by circularly polarized radiation of 23 eV energy from a thick rubidium layer adsorbed on a platinum single crystal [47]. Upper part: photoelectrons leaving a $p_{3/2}$ or $p_{1/2}$ hole state of opposite spin polarization with a fit using the atomic model (curves). Lower part: Auger electrons. The rectangles describe the experimental uncertainties. The two curves describe the upper and lower limits in application of the atomic model predicted using the data of the photoelectron spin polarization of the upper part under the assumption of a singlet coupling of the Auger decay. From [47].

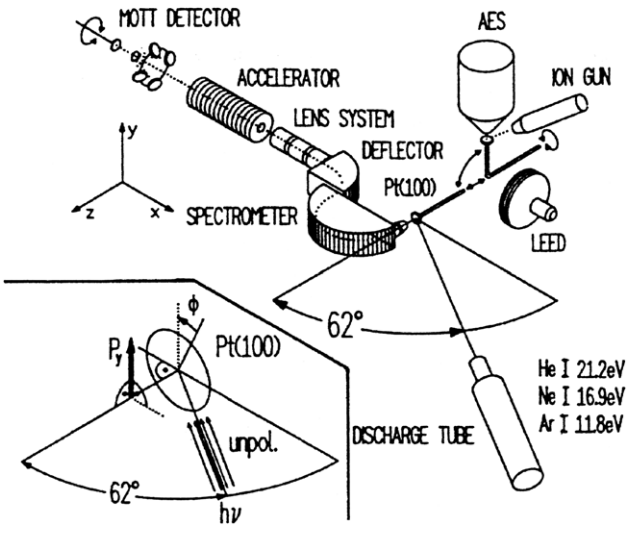

Figure 20. Experimental set-up [48–50]. AES and LEED as in figure 6. From [48].

spin polarization. Two components of the spin polarization vector were simultaneously measured, the horizontal one perpendicular to the crystal surface P_z and the vertical one in

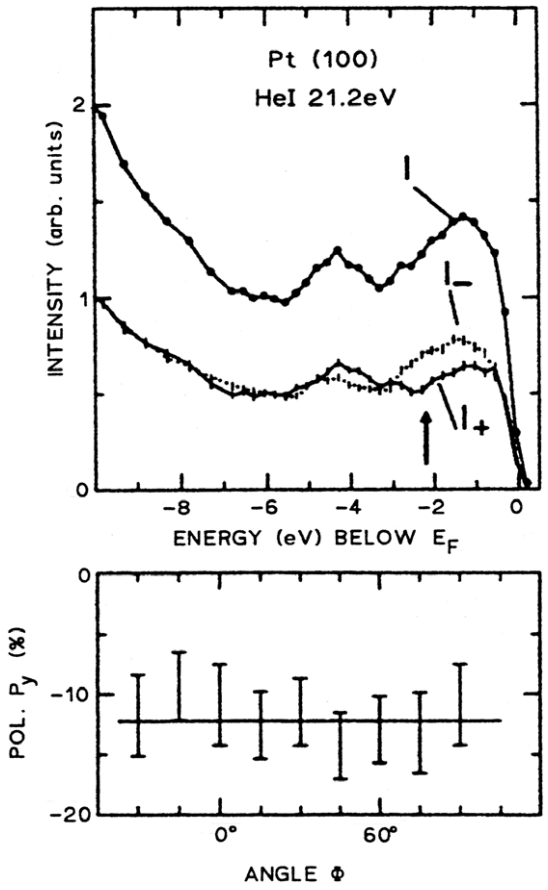

Figure 21. Top: photoemission spectrum obtained with unpolarized HeI radiation for normal emission from a 1 × 1 surface of Pt(100) [48], see figure 20. I denotes the total intensity, and I_+ and I_- the partial ones with spin up and down, respectively. The arrow at −2.2 eV indicates the energy for which the ϕ dependence of $P_y = P_\perp$ was determined (lower part). ϕ is the azimuthal angle of the crystal rotation about the surface normal. From [48].

the crystal surface plane P_y perpendicular to the reaction plane (photon momentum, electron momentum). In all cases studied so far at Pt(100) [48] Pt(110) [49], Pt(111) and Au(111) [50] the spin polarization component P_z has been measured to be zero for all photon energies, photoelectron energies and azimuthal angles ϕ.

The spin polarization component $P_y = P_\perp$, however, has been measured to be about −10% to −20% for Pt(100), Pt(111) and Au(111) for photoelectrons arising from the first band below the Fermi energy for all azimuthal angles ϕ as given in figure 21. The measurement with Pt(110), however, showed an additional effect: an oscillation of the spin polarization component around the average value of −10% with azimuthal rotation of the crystal about the crystal normal: the spin polarization oscillates from zero up to −20% as given in figure 22, reaching an average value of −10% at $\phi = 45°$ and 135°[49]. This indicates an answer to the question as to where this additional spin polarization effect might have its origin: Pt[110] has aligned rows of platinum atoms in its surface which bring an additional quantization axis into the description of a reaction plane in photoemission. As discussed in section 3, in atomic photoionization the

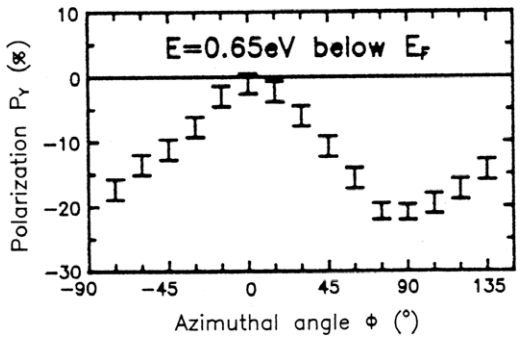

Figure 22. Dependence of the spin polarization $P_y = P_\perp$ on the rotation ϕ of the Pt(110) crystal about the surface normal ($\phi = 0°$: missing rows perpendicular to the reaction plane) [49]. Adapted from [49].

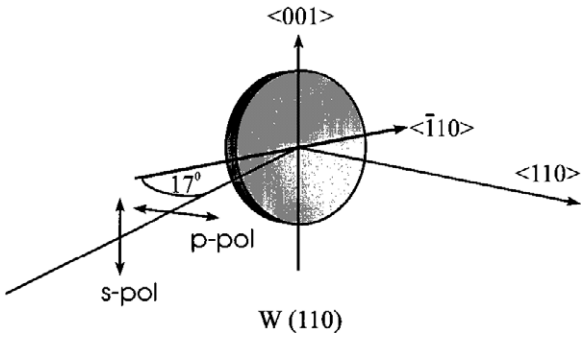

Figure 23. Experimental set-up of [51]. The light impinges onto the tungsten surface under a grazing angle of 17°. The electrons are collected in normal emission. The spin polarization $P_\perp$ is measured parallel to the [001] direction. Reproduced with permission from [51]. Copyright 1996 American Physical Society.

reaction plane refers to the photoelectron momentum as well as to the photon momentum and the electric vector of the radiation for unpolarized and linearly polarized radiation, respectively. This gives rise to the question as to whether one of these quantization axes has to be replaced by a target alignment direction with respect to the so-called dynamical spin polarization of photoelectrons $P_\perp$ ejected by unpolarized or linearly polarized radiation.

In order to study this in more detail, linearly polarized radiation was used: figure 23 shows the experimental set-up of the Kisker group [51]: s- or p-linearly polarized radiation hits the (110) surface of a tungsten crystal off-normally; the spin polarization component $P_\perp$ parallel to the [001] direction was measured to be zero for s-polarized light but different from zero for p-polarized light as shown in figure 24. This result can be easily understood. For s-linearly polarized radiation there is no spin polarization component parallel to the E vector according to equation (3). For p-polarized light the spin polarization component measured stood perpendicular to a plane with all three directions: light polarization, photoelectron momentum and alignment of the crystal surface in the [1$\bar{1}$0] direction. It is worth noting that in figure 25 the spin polarizations show opposite signs in the $4f_{5/2}$ and $4f_{7/2}$ peaks of tungsten, demonstrating the spin–orbit interaction being responsible for the spin polarization effect measured: again, had no electron spectrometer been used to resolve the two fine structure split f-peaks in the photoelectron spectrum, the spin polarization effect would have disappeared because the spin polarizations of both peaks would have canceled each other out. Furthermore the authors [51] compared the energy dependences of the measured spin polarizations with values expected within the atomic picture, as shown in figure 25, and found a good agreement.

An angle- and spin-resolved photoemission experiment with Pt(110) was performed under the high symmetry of normal incidence and normal emission [52] as given in figure 26 in order to study whether the crystal alignment, the linear photon polarization or the photoelectron momentum are the corresponding directions to define a reaction plane, where the spin polarization vector stands perpendicular in photoemission with linearly polarized radiation. The spin polarization P_z measurement took place perpendicular

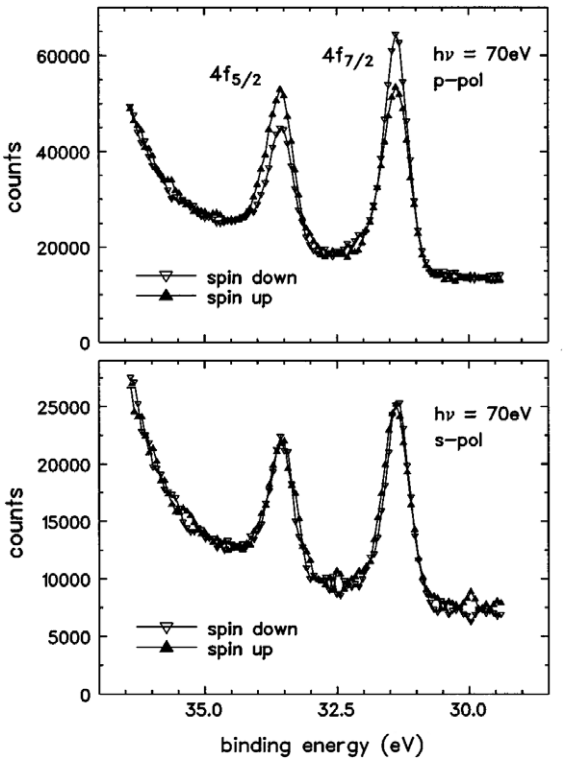

Figure 24. Spin-resolved W 4f photoelectron spectra for 70 eV photon energy according to figure 23. The open triangles mark the spin-down channel (antiparallel [001]) and the filled triangles the spin-up channel (parallel [001]). While the use of p-linearly polarized light (upper panel) yields spin polarized photoelectron peaks, with s-polarized light no polarization occurs [51]. Reproduced with permission from [51]. Copyright 1996 American Physical Society.

with respect to the crystal surface. This polarization is perpendicular to the plane defined by the surface alignment [1$\bar{1}$0] and the electric vector of the radiation and has its maximum in a crystal rotation diagram measured by varying the azimuthal angle ϕ about the crystal normal at $\phi = 45°$ and 135° according to equation (3), see figure 27 (left part). This clearly demonstrates the importance of the target alignment together with the E vector of the radiation used to define the reaction plane.

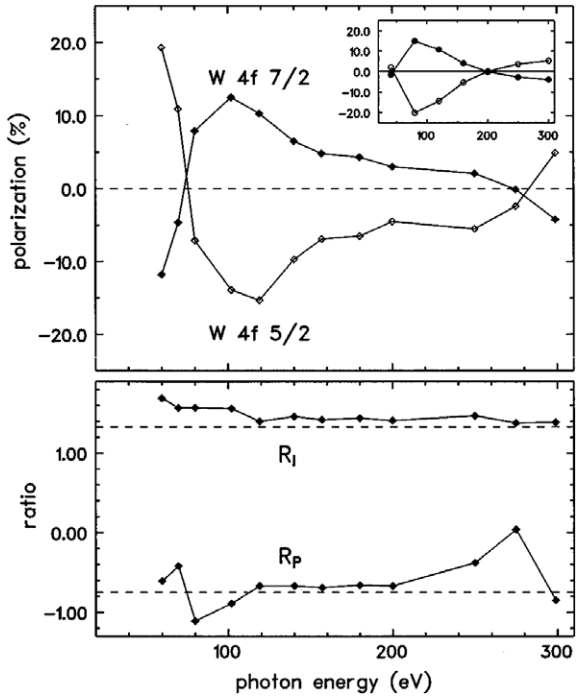

Figure 25. Upper panel: photoelectron spin polarization $P_\perp$ of the spin–orbit split tungsten 4f sublevels of W(110) in cross-comparison with the case of free atoms (inset). The lower panel shows the ratios of $j = 7/2$ and $5/2$ for polarization R_p and intensity R_I in cross-comparison with free atoms (dashed lines) [51]. Reproduced with permission from [51]. Copyright 1996 American Physical Society.

Using equation (4) the reason for the existence of such a spin polarization component is identified: a phase shift of two complex matrix elements defining two outgoing partial waves leaving the crystal in two different hole states with identical energy as shown in figure 27 (right part). The two complex transition dipole matrix elements have been identified to describe the transition from initial Σ_5^4 and Σ_5^3 bands at the X-point of the band structure calculated by Noffke [53, 54] in the hybridization region as given in figure 28. It is worth noting that the quantum mechanical interference of two outgoing partial waves describing the photoelectrons which result in a spin polarization perpendicular to the reaction plane is, of course, a final state effect, although the corresponding bands which show hybridization are initial bands in figure 28. However, this band structure describes initial and hole states in a one-electron picture like the orbitals in molecules. Initial states are calculated in a ground state calculation but the hole states—identical with the initial states only in the one-electron picture—only exist after the photoemission process. Hole states are thus always final states for the whole many-electron system like the p-holes in the photoionization of rare gas atoms are final ionic states $^2\mathrm{P}_{1/2}$ or $^2\mathrm{P}_{3/2}$, as discussed in section 2. The hybridization of the hole states creates complex matrix elements and thus phase shifts and a quantum mechanical interference in the final states with the consequence of the photoelectron spin polarization $P_\perp$.

5. The relationship between photoemission phase shifts and time delays in attosecond-resolved photoemission

The phase shifts measured in spin-resolved photoemission as explicitly shown in figures 16 and 27 may be interpreted as different delays of partial photoelectron wavefunctions with respect to the time the photoelectron leaves the atom or solid from where it comes. In 2007 the first real attosecond time-resolved photoemission experiment in condensed matter with ultrashort XUV laser pulse radiation was performed on W(110) [55], after a corresponding attosecond-resolved

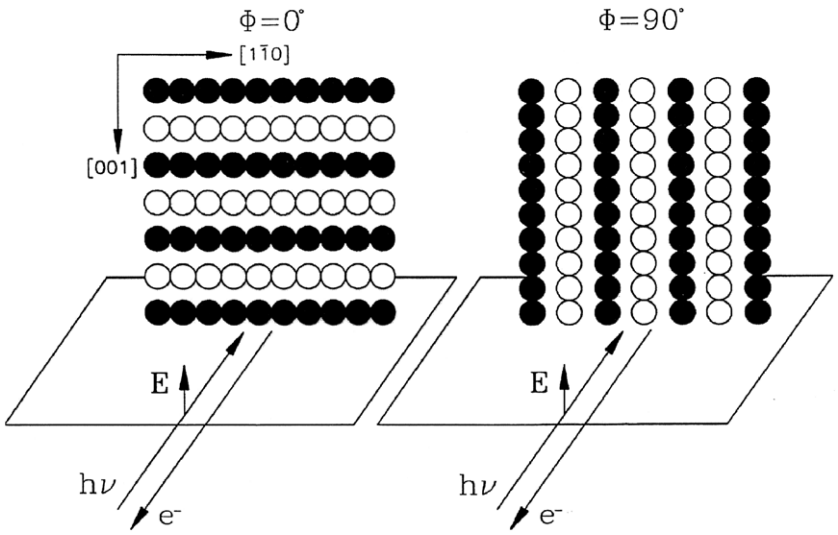

Figure 26. Scheme of the angle-resolved photoemission experiment in normal incidence and normal emission at the reconstructed Pt(110) (1 × 2) surface, the so-called 'missing-row model' of reconstruction and definition of the azimuthal angle ϕ. For $\phi = 0$ the electric vector E of linearly polarized radiation is perpendicular to the close-packed rows in the [1$\bar{1}$0] direction, while for $\phi = 90°$ it is parallel to the [1$\bar{1}$0] direction [52]. From [52].

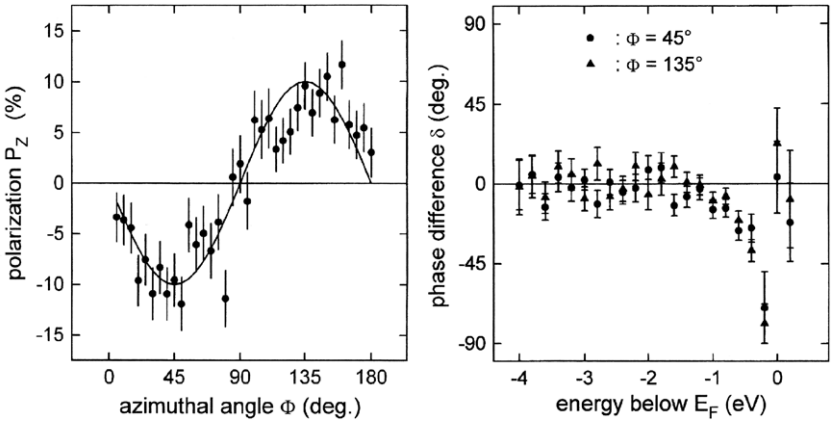

Figure 27. Left part: spin polarization $P_z = P_\perp$ of photoelectrons emitted by linearly polarized radiation (11.8 eV) from Pt(110) in normal incidence and in normal emission (electron binding energy 0.5 eV) as given in figure 26 as a function of the azimuthal angle ϕ, the crystal is rotated about its normal. Right part: experimental values of the phase difference δ between the complex transition dipole matrix elements M^3 and M^4 versus binding energy for a photon energy of 11.8 eV according to the transition shown in figure 28 as an arrow. The phase shift has been obtained from the measured spin polarization [52]. From [52].

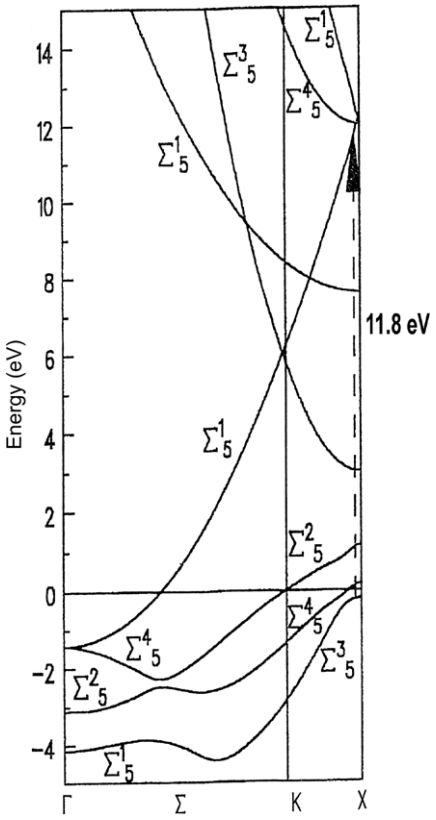

Figure 28. Band structure calculation of Pt(110) by Noffke [53, 54] concerning the transition (given as an arrow) discussed in figure 27. From

photoionization spectroscopy measurement by use of the streaking technique using an ultrashort near-IR light pulse with a stabilized carrier envelope phase as a clock took place successfully with free atoms [56]. Since the duration of the photoelectron pulse (300 as) was short compared with the oscillating period of the IR pulse (2.3 fs), the photoemitted electrons were accelerated or decelerated like ballistic particles by the phase-stabilized, non-jittering electric field of the IR pulse. Figure 29(a) shows the experimental raw streaking spectrum of normal photoemission of W(110), where the 300 as 91 eV XUV pulse and the collinearly propagating linearly polarized IR pulse hit the surface under the Brewster angle such that the IR E vector is nearly parallel to the surface normal. The kinetic energies of the photoelectrons emitted from the 4f core level at about 55 eV and from the d conduction band at about 87 eV strongly oscillate over about 10 eV with the electric field of the IR beam, if the delay between the XUV and the IR pulses is varied. These raw data as well as the smoothed and interpolated streaking spectrum in figure 29(b) using the center of masses of 4f and conduction band peaks and the corresponding fit given in figure 29(c) exhibit a delay between the escape times of photoelectrons through the surface for the different photoelectrons from the 4f and the conduction band to be 110 ±70 as [55].

This delay observed experimentally for the first time may have different reasons since the electrons have different kinetic energies and they may originate from locations at different distances with respect to the surface. Five different theoretical approaches to describe the dynamics of the photoemission process at W(110) exist so far, all yielding delays between 42 and 110 as for the core and the conduction band electrons photoemitted. The first theoretical approach by Echenique used a static band structure calculation as given in figure 30 [55] and explained the different delayed emission by different group velocities of the final states given as slopes dE/dp with $p = kh/2\pi$ as the electron momentum, in good agreement with the experiment. The critical point of this approach was, of course, the use of a static band structure which might not be valid for an ultrashort photoemission process.

By taking the delocalization of the 4f and 5d states of tungsten into account differently, using a quantum mechanical approach and assuming that the IR laser radiation does not penetrate into the crystal, Kazansky and Echenique [57] found that the concept of group velocities could be ruled out for small time intervals. The main effect of the delay is attributed to the localized nature of the core electrons in contrast to the

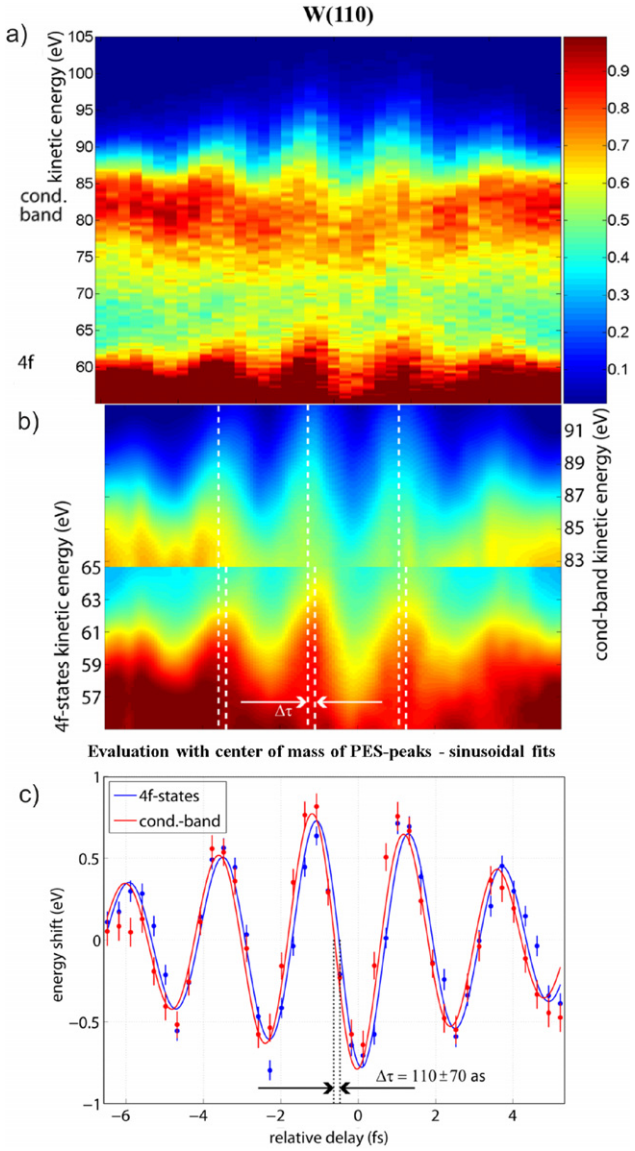

Figure 29. (a) Raw streaking spectrum of W(110): the dependence of photoelectron kinetic energy as a function of the delay between the IR and the 91 eV XUV pulse. The photoelectrons from the 4f core states and from the d conduction band close to the Fermi energy follow with their energies the oscillation of the electric field of the IR pulse [55]. The photoelectrons ejected by the as-XUV pulse leave the crystal in normal photoemission parallel to the E vector of the fs-IR pulse. (b) Smoothed streaking spectrum of W(110) after cubic spline interpolation of the oscillation of the kinetic energies as given in (a) as a function of the delay between IR and XUV pulse [55]. (c) Fit through the streaking oscillations in (b) at the center of mass of the 4f state peak and of the conduction band peak. They are shifted in delay by 110+/−70 as [55]. The photoelectrons leave the crystal surface at different times. Adapted from [55].

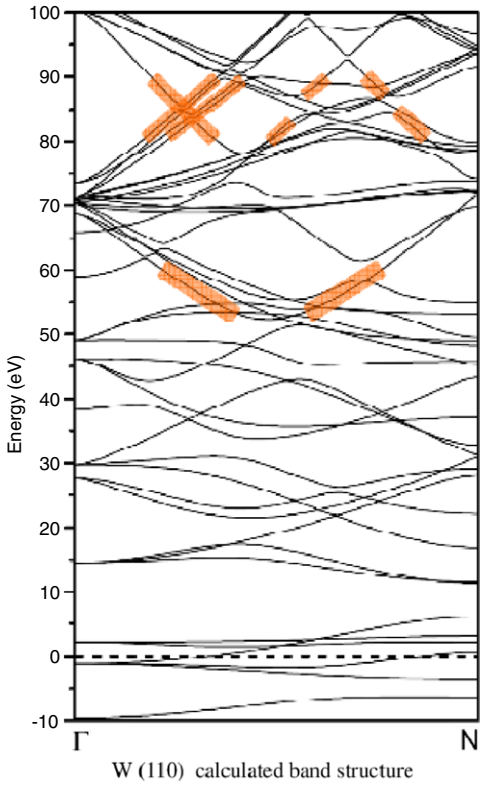

Figure 30. Static band structure calculation of bcc tungsten along ΓN momentum direction [110]. Zero on the energy axis is the Fermi energy. Electrons from the 4f states are photoexcited by the 88–94 eV XUV peak into the upper conduction band that is shaded and centered at about 58 eV. Similarly, electrons from the conduction band reach bands with energy around 85 eV. The slope of the upper conduction bands estimates the group velocities of the electrons inside the crystal [55].

conduction band electrons which are completely delocalized. In contrast to this approach Baggesen and Madsen [58] found in a quantum mechanical approach by use of Volkov waves as final states that the delay originates from the travel through the surface. Zhang and Thumm [59] assumed a localized core state and delocalized electrons in the conduction band in a jellium approximation under the circumstances that the streaking laser field inside the solid is included. The photoemission by XUV was dealt with by the first-order perturbation theory, whereas the streaking itself was not dealt with by perturbation; they took into account interfering contributions from different lattice layers to the dipole matrix elements of the optical transition under the circumstance that the core electrons were delocalized within the jellium model. They calculated a delay of 110 as, in agreement with the experiment. Lemell *et al* [60] used a classical transport theory, neglected a penetration of the IR laser field into the crystal but used different group velocities for electrons from 4f, 6s and 5d states. They found a delay of 110 as, in agreement with the experiment with group velocities as given in [55] or alternatively 42 as with a free-particle dispersion relation. Summarizing, with the given theoretical approaches so far the real nature of the delay is not yet quantitatively understood. There is, however, no doubt that it exists: electrons of different states excited by an ultrashort attosecond pulse leave the crystal surface at different times.

The fact that electrons from different bands with different symmetries, i.e. orbital angular momenta (s, p, d, f) may have different group velocities, even if they have the same kinetic energies [60], gives rise to the general question as to which parts of the full Hamilton operator influence the

time delays of emitted photoelectrons measured by means of streaking experiments. Very recently Zhang and Thumm [61] discussed theoretically the relationship of streaking and Wigner time delays. Based upon the essence of the time delay introduced by Wigner and Smith [62, 63] they discussed theoretically how phase shifts of individually traveling plane wave components lead to spectral delays: $\tau = \mathrm{d}\varphi/\mathrm{d}\varepsilon$ with τ being the Wigner time delay, φ the phase shift and ε the photoelectron kinetic energy. The Wigner relationship is based upon the definition of the group velocity mentioned above, $\upsilon = \mathrm{d}E/\mathrm{d}p$. This means in practice that a delay of photoelectron wavepackets t is given by the derivative of the phase shift φ to the electron energy as being $t = 658\,\mathrm{as} \cdot \mathrm{d}\varphi/\mathrm{d}E$ with E in units of electronvolts. Phase shifts φ between different partial waves thus automatically create a delay of the electron wavepackets $t_1 t_2$ if they show a different dispersion $t_1 - t_2 = 658\ \mathrm{as}\,\mathrm{d}(\varphi_1 - \varphi_2)/\mathrm{d}E$. This result stimulates the question how phase-shift-resolved photoemission experiments can be performed in reality.

Indeed, phase-shift-resolved photoelectron emission experiments have been successfully performed with free atoms and molecules, adsorbates and solids in past decades as described in detail in sections 3 and 4. The results for the xenon atom are shown in figure 16. The slope of the measured phase shift difference curves as a function of the energy $\mathrm{d}(\delta_\mathrm{d} - \delta_\mathrm{s})/\mathrm{d}E$ directly gives the time delays of the photoelectrons emitted in the individual continuum channels

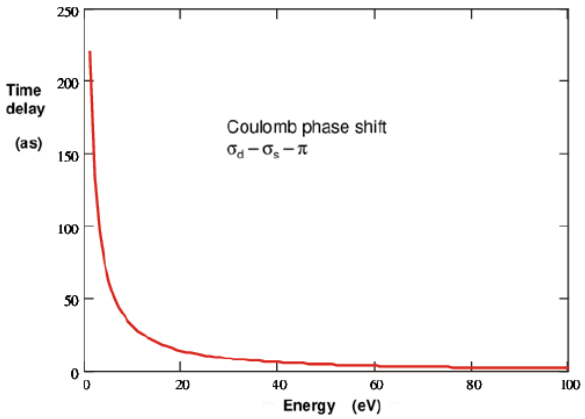

Figure 31. Analytically calculated energy dependence of the energy slope of the Coulomb phase shift $\sigma_\mathrm{d} - \sigma_\mathrm{s} - \pi$ given as Wigner time delay (see text).

d and s to be 45 as for the Coulomb phase shift alone and 76 as = 45 + 31 as in total at the kinetic energy of 7 eV (20.5 eV photon energy) in figure 16. Figure 31 shows that the time delay due to this Coulomb phase shift strongly decreases with increasing kinetic energy and is negligible (<8 as) for kinetic energies higher than 30 eV. With respect to the time-resolved photoemission of f core level bands and of the conduction band of W(110) discussed above

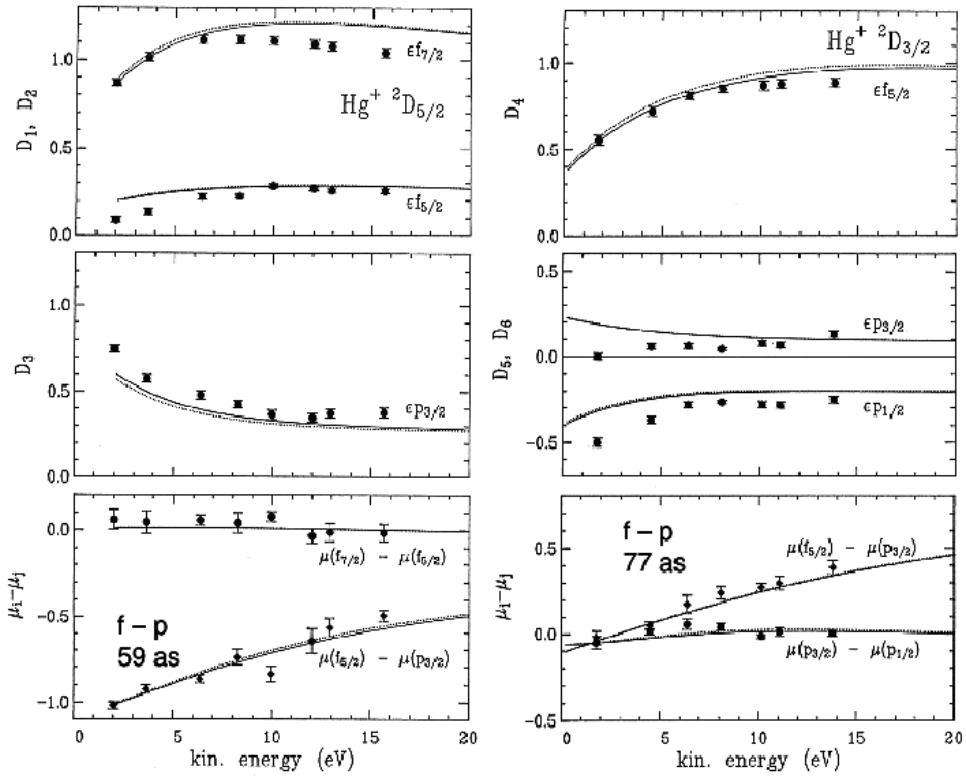

Figure 32. Matrix elements D and phase shift differences $\mu = (\delta - \sigma)/\pi$ in units of π, without Coulomb phases σ, for f and p photoelectrons, leaving the mercury atom back in the 5d $^2D_{5/2}$ (left part) and 5d $^2D_{3/2}$ (right part) final ionic state, experiment (error bars) and theory [64], as a function of the photoelectron kinetic energy. The numbers denote the corresponding Wigner time delays given by the slopes of the phase shift curves. Adapted from [64].

figure 32 (both lowest parts) shows the measured phase shift differences of $f_{7/2}$ and $f_{5/2}$ continuum waves with respect to a $p_{3/2}$ continuum wave obtained in spin-resolved photoelectron emission of mercury atoms together with the corresponding matrix elements [64]. Note that the phase shifts given describe only the non-hydrogenic part, after the Coulomb phase shifts have been subtracted; they are given as differences of quantum defects $\Delta\mu$ in units of π [41]. In the energy range presented in figure 32 the non-Coulombic phase shift differences have a slope which defines a time delay between f and p waves to be 77 as and 59 as for the Hg atoms $d_{3/2}$ and $d_{5/2}$ initial states, respectively. It is worth being noted that the phase shift differences $f_{7/2} - f_{5/2}$ as well as $p_{3/2} - p_{1/2}$ in figure 32 do not show any dispersion, with the consequence that the spin–orbit interaction in the final state alone as a part of the total potential, in which the photoelectron leaves, does not create any time delay. Obviously the main part of the time delay with respect to f and p waves are due to the different centrifugal term $l(l+1)/r^2$ in the Schrödinger equation.

In the photoemission of metal surfaces there is the prominent showcase example of a pronounced dynamical spin polarization $P_\perp$ and thus of a large phase difference and time delay: in the photoemission of Pt(110) in normal electron emission and in normal incidence of linearly polarized radiation as given in the right part of figure 27 [52]. Its slope versus energy gives the high value of 4.7 fs for the Wigner time delay of electrons from the two bands Σ_5^3 and Σ_5^4 [52–54]. This value of a time delay for photoelectrons from different bands is so high because the kinetic energy of the photoelectrons is low and the two bands show a strong hybridization.

Phase-shift-resolved photoemission by means of spin polarization measurements of photoelectrons may give access to time delays seen in an as-time-resolved photoemission experiment. The derivative of the phase shift to the photoelectron kinetic energy is directly related to the time delay as given by the Wigner relationship mentioned.

6. Photoelectron spin polarization with chiral targets

Normal incidence of linearly polarized light at centrosymmetric cubic crystals and normal photoelectron emission was assumed to yield spin polarization only if the target is aligned like a (110) surface with atomic chains in-plane as discussed already in section 4 [7, 25]. Tamura *et al* [65] refuted this belief and predicted normal emission photoelectron spin polarization by linearly polarized light for (111) surfaces of fcc crystals. Their predictions were based upon a one-step photoemission theory using a relativistic multiple scattering formalism and they identified the spin–orbit interaction as its main cause: photoelectrons can only be polarized perpendicular to a mirror plane. Schmiedeskamp *et al* [66] performed a corresponding spin-resolved photoemission experiment with Pt(111) in normal incidence of linearly polarized radiation and normal photoelectron emission. Figure 33 shows the experimental results [66] in cross-comparison with the theoretical prediction [65], both in excellent agreement.

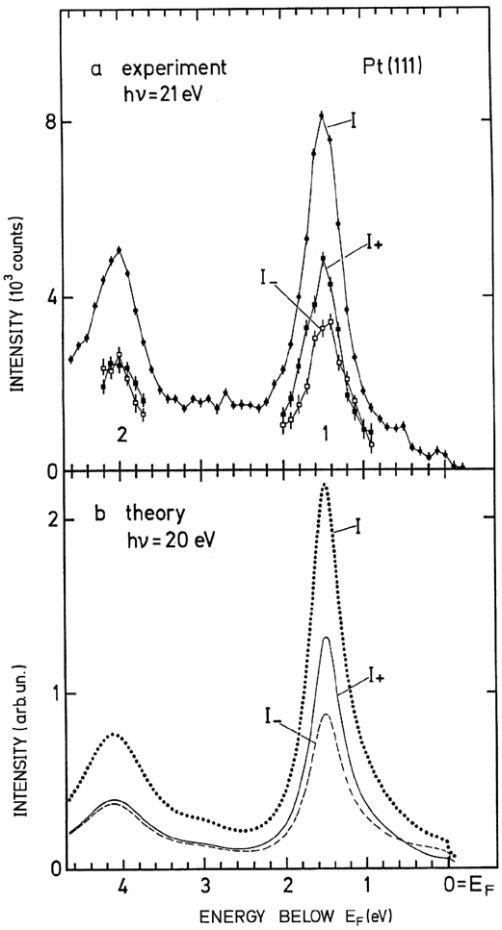

Figure 33. Photoelectron spectrum obtained from normal incidence of linearly polarized light and normal photoelectron emission. The partial intensities I_+ and I_- correspond to spin directions parallel and antiparallel to a trace of non-mirror plane in the Pt(111) surface, experimental results [66] (a) and calculation [65, 66] (b). The corresponding experimental set-up is given in figure 34. From [66].

Figure 34 demonstrates that, according to the measurements, the spin polarization vector rotates in the plane parallel to the surface three times faster than the rotation of the crystal about its normal. When the crystal is rotated about 15° the spin polarization rotates 45°; the data show a periodicity of 120°. This is typical for the threefold symmetry of a fcc crystal with respect to the ⟨111⟩ directions. Unlike hcp crystals, fcc crystals are close packed with a packing sequence ABCABC instead of ABAB for hcp. This ABC sequence together with the E vector of the radiation lying in the surface plane describes a screw and gives the (111) surface a helicity; although it has not been experimentally verified the authors of [65, 66] supposed that an ultrathin double layer of Pt(111) AB would not create spin polarized photoelectrons comparable to those shown in figures 33 and 34.

It is worth noting that it has been well known since 1995 [67–69] that chiral structures influence the spin polarization of elastically scattered electrons. In photoemission an asymmetry in the angular distribution of photoelectron emission from chiral molecules induced by circularly polarized light has been experimentally

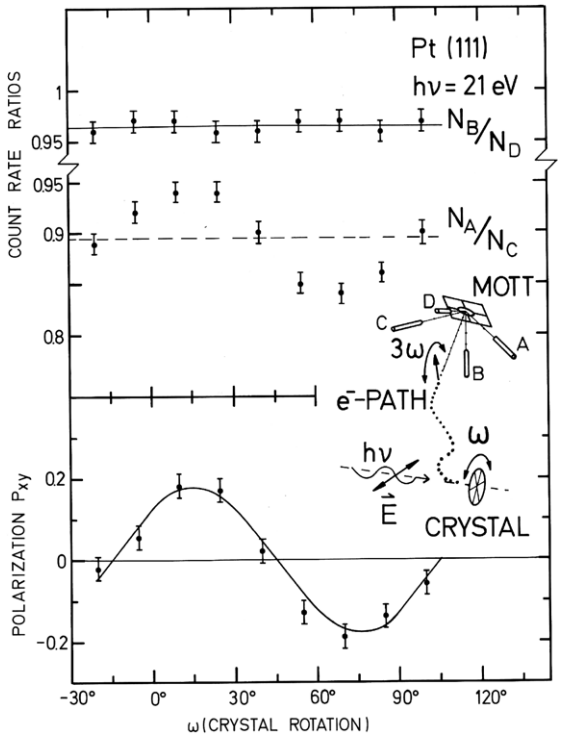

Figure 34. Photoelectron spin polarization P_{xy} in the first peak of figure 33 for normal linearly polarized radiation incidence and normal photoelectron emission. Top: ratios of the Mott-detector count rates N_A/N_C and N_B/N_D versus the rotation angle ω about the Pt(111) surface normal. Inset: relation of spin polarization directions and Mott-counter arrangement. The spin polarization vector rotates in a plane parallel to the surface three times faster than the rotation of the crystal about its surface normal [66]. From [66].

identified [70]. Finally, recently Göhler *et al* [71] studied the spin selectivity in electron transmission through self-assembled monolayers of double-stranded DNA adsorbed on an Au(111) crystal serving as a phototarget for the spin polarized photoelectrons.

7. The Rashba effect as a reason for spin polarized photoemission

The previous sections primarily dealt with how the photoemission process can induce a polarization of the photoelectrons due to spin–orbit interaction. In the condensed matter jargon this is commonly referred to as 'final state effects' or 'matrix element effects of optical transitions (optical pumping)'. In this section it will be shown that the spin–orbit interaction can also induce a momentum-dependent spin polarization of the so-called initial states. Further it will be shown that for a typical spin- and angle-resolved photoemission spectroscopy (SARPES) measurement of delocalized states both initial and final state effects have to be taken into account in order to fully understand the data. Here the aim is to put the results obtained for Rashba systems in the general perspective of spin–orbit interaction-induced spin effects in photoemission. A more extensive review of spin-resolved photoemission on Rashba systems has recently been given in [12].

The existence of a surface of a crystal in angle-resolved photoemission automatically means a breaking of the inversion symmetry at the surface. For an electron with a momentum k and a spin s space inversion symmetry means that it is equivalent whether the electron moves into one direction with k or in the opposite with $-k$, i.e. $E(k, s) = E(-k, s)$. Time inversion symmetry in the cases of non-magnetic material means $E(k, s) = E(-k, -s)$. In the bulk of a non-magnetic centro-symmetric three-dimensional crystal $E(k, s) = E(k, -s)$ is thus valid, resulting in the spin degeneracy of the initial states. At the surface of a crystal or for crystals lacking an inversion symmetry center, this symmetry is broken and a polarization of the bands is allowed. For crystals lacking an inversion symmetry center in the bulk this is called the Dresselhaus effect [72], whereas at the surface, or more generally for a inversion symmetry breaking along the z direction of the crystal, the resulting spin polarization is referred to as the Rashba effect [73].

That for the Rashba effect the bands actually become spin polarized can be understood by the following simple argument. The sudden termination of the crystal at the surface results in a sudden change of the potential. In the rest frame of an electron moving parallel to the surface, i.e. an electron in a two-dimensional electron gas, this potential gradient is transformed in a magnetic field. The size and sign of this magnetic field, of course, depend on the velocity and direction of motion of the electron. This magnetic field in the rest frame of the electron causes a Zeeman splitting of states with spin parallel or antiparallel to the magnetic field, where the size of the splitting increases for increasing in-plane momentum. For electrons with opposite momentum the sign of the magnetic field and thus also of the splitting is reversed. For a free-electron-like parabola this results in the famous momentum shifted parabolae as observed for the Au(111) surface state by LaShell *et al* [4]. That these states actually have opposite spin direction in agreement with the above argument was verified by SARPES by Hoesch *et al* as depicted in figure 35 [74–76]. Similar behavior has been experimentally and theoretically studied for Bi surfaces [77, 78].

Although the hand-waving explanation given above qualitatively reproduces the spin structure of simple free-electron-like systems, it fails to reproduce the observed splitting quantitatively or to predict the spin structure of more complex systems. In this respect it is more appropriate to consider a model initially described by Bihlmayer *et al* [79] and later revisited by others [80] where the charge density distribution around an atom core is considered. At each atomic layer a local atomic contribution to the spin splitting arises in the vicinity of the nuclei according to the form

$$\Delta E \propto k_{\parallel} \int_{\Delta z} \mathrm{d}z \, \frac{\partial V}{\partial z} |\Psi(z)|^2. \qquad (6)$$

Here V is the spherical Coulomb potential of the nuclei and Ψ the wavefunction of the spin-split state. It has been shown that more than 90% of this contribution arises within $\Delta z \approx 0.5$ a.u of the nuclei, where the antisymmetric Coulomb gradient $\partial_z V$ is most significant [79]. The spin splitting as measured by photoemission is then the sum of

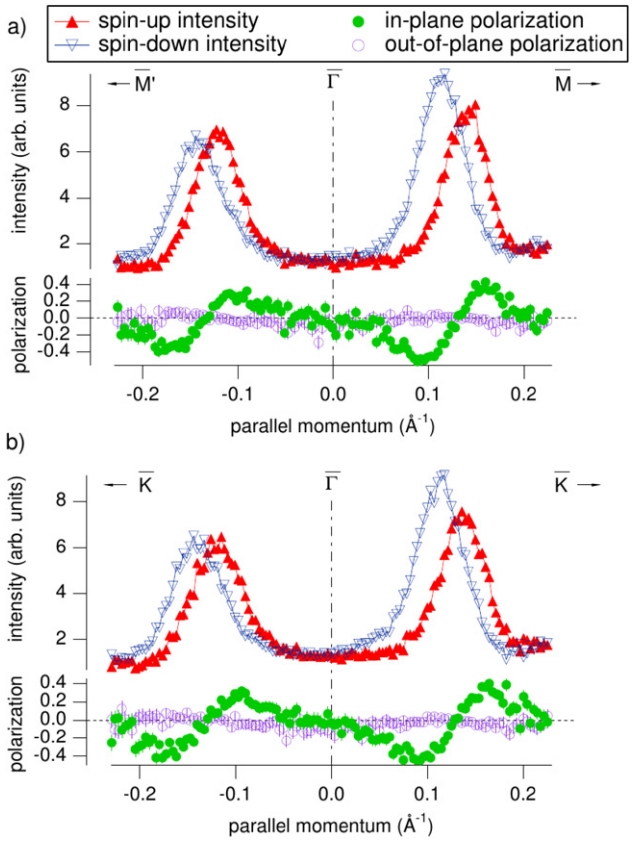

Figure 35. Measured spin-resolved momentum distribution curves at binding energy 170 meV on Au(111) using linearly p-polarized uv light of 21 eV for ΓM (a) and ΓK (b) directions. The lower parts show the measured transverse spin polarization components [74]. Reproduced with permission from [74]. Copyright 2004 American Physical Society.

the contributions from all layers where the wavefunction penetrates. Without going into too much detail it is clear that, when the wavefunction distribution is symmetric around the atom core, the resulting splitting is zero. If the symmetry of the wavefunction distribution is broken a spin splitting directly occurs, where the magnitude and the sign of the splitting are given by the local slope of the wavefunction. Furthermore, a three-dimensional equivalent of this model also reproduces changes of the spin quantization axis away from purely along the y direction. If the asymmetry is solely along the z direction the spin quantization axis is along the y axis, if an additional in-plane symmetry breaking is present along the x direction this results in an out-of-plane spin component. This threefold-symmetric out-of-plane spin polarization was first predicted and also experimentally observed for the long range ordered surface alloy of Bi on Ag(111) as shown in figure 36 [81, 82]. Furthermore it is worth noticing that the states do not necessarily have to be purely two-dimensional. On vicinal Au(111) surfaces it was found that the spin structure can be described along the same lines as for the flat surface and that the steps do not influence the splitting or degree of polarization as long as the wavelength of the states is shorter than the step size. After this transition the splitting even increases due to the fact that the wavefunction experiences a larger corrugation and thus a larger asymmetry [83]. Also for the one-dimensional states of Au on Si(557) [84, 85] and for Bi(114) [86] a Rashba-type spin splitting has been observed showing the general nature of the Rashba model.

Within this model it is also possible to achieve a reversal of the spin direction if the contribution from the individual layers does not have the same sign or if the asymmetric wavefunction distribution is opposite to that for a standard Rashba system. The latter situation is responsible for the reversal of the spin structure of the Gd(0001) surface state after oxidation [87] and has also been predicted to be the origin of the similar constant energy spin structure of the electron-like Au(111) surface state and the hole-like surface states on long range ordered Bi, Pb, or Sb surface alloys on Ag(111) and Cu(111) [88, 89]. The first of the described origins of a spin structure reversal can occur in quantum well states formed in thin metal films, such as, for example, Pb on Si(111) [90–93]. These states are best described by a rapidly oscillating Bloch wave determined by the atomic structure modulated by the quantum well envelope function [94, 95]. Because the barriers of the quantum well are not infinite the wavefunction will spill across it and at every layer the minimum of the probability density will shift away from the core positions, resulting in a contribution to the spin splitting according to equation (6). For the realistic asymmetric confinement conditions induced by the difference between the metal–vacuum and the metal–substrate interface not all contributions to the Rashba splitting will cancel and a net spin splitting will be observed. For Pb films grown on the $(\sqrt{3} \times \sqrt{3})$ Pb reconstructed Si(111) substrate it is actually found that the negative contributions beat the positive contributions, resulting in a negative spin splitting and thus a reversal of the spin orientation compared to the Au(111) surface state as shown in figure 37 [96]. In a follow-up experiment for Pb films grown on a Bi reconstructed Si(111) substrate [97] it was found that it is actually possible to change the Rashba splitting of the quantum well states through changes in the interface and to induce an out-of-plane polarization component [98]. These observations can only be explained within the wavefunction distribution model described here.

The spin structure of the recently discovered three-dimensional topological insulators [99] is directly related to the Rashba-type spin structure discussed above, but with some important differences. Whereas for the trivial Rashba systems described above the surface states are typically in a projected bulk bandgap, the surface states of a topological insulator are in a parity inverted absolute bulk bandgap. Within a simple band structure picture this parity inversion also causes the outer branch of the spin-split states to bend down again and connect to the valence band whereas the inner branch connects to the conduction band. Although it does not grasp the parity inversion of the bulk bands it is possible to describe the transition from a Rashba-type band to a topological state through a continuous tight-binding model by just varying an anisotropy parameter [100]. The similar background in the spin–orbit interaction and symmetry breaking of Rashba and topological states also becomes clear when considering the surface state band structures of Sb(111), $Bi_{0.9}Sb_{0.1}$(111) and

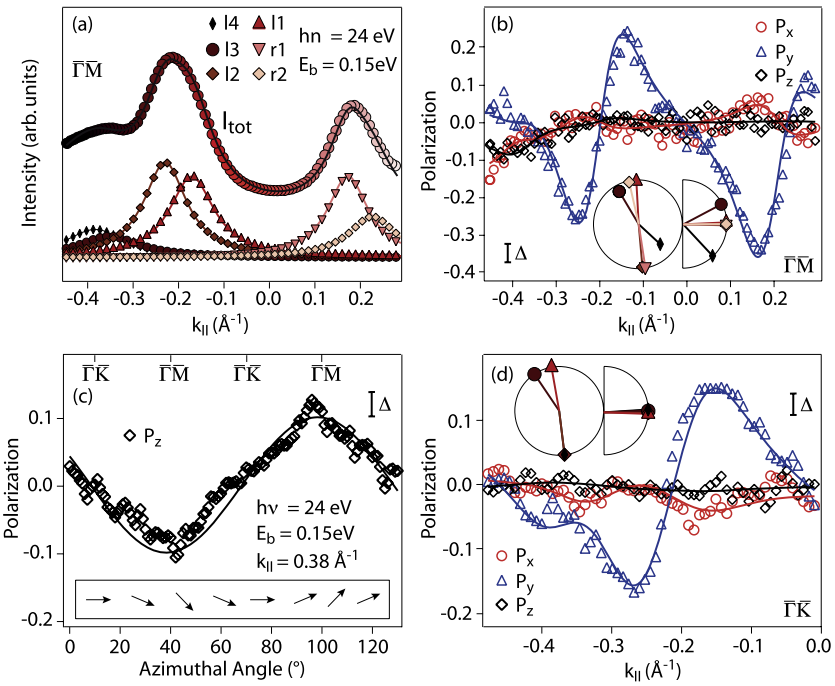

Figure 36. SARPES data obtained for the long range order surface alloy Pb/Ag(111) with $h\nu = 24$ eV at $E_b = 0.15$ eV. (a) Measured MDC in the ΓM direction, showing also the fitted peaks. (b) Measured (symbols) and fitted (solid lines) spin polarization data. (c) Measured out-of-plane spin polarization (symbols) obtained from an azimuthal scan at $k_\parallel = 0.38$ Å^{-1}, approximately showing a sinelike behavior with $2\pi/3$ periodicity (solid line). The inset visualizes the out-of-plane rotation as a function of the azimuthal angle. (d) Spin polarization for a MDC in the ΓK direction. The insets in (b) and (d) show the obtained spin polarization vectors [82]. From [82].

Bi(111). The first two materials are topologically non-trivial with $Bi_{0.9}Sb_{0.1}$ being the first three-dimensional topological insulator [101, 102] and the latter is a prototypical Rashba system [77]. However, the surface states and their spin structure of all materials is almost completely identical.

The next generation of topological insulators consisting of Bi_2Se_3, Bi_2Te_3 and Sb_2Te_3 only has a single spin polarized Dirac cone at the surface [103, 104], resulting in just a single spin polarized band crossing the Fermi level [105]. The spin direction is like for the Rashba systems directly locked to the momentum and the primary spin quantization axis lies in the surface plane perpendicular to the in-plane momentum. However, upon a more detailed consideration the situation is more complex. A constant energy surface of, for example, Bi_2Te_3 is highly warped and, depending on the exact binding energy, goes from circular to hexagonal to snowflake-like. Fu has shown that this warping can be reproduced by including third-order terms in k in the tight-binding Hamiltonian and predicted that this warping should result in an out-of-plane spin polarization of the initial state with a threefold symmetry [106]. As reproduced in figure 38 this has been verified by SARPES measurements of the topological state at the Fermi level, where the out-of-plane polarization reverses sign when rotating the sample by 60° and goes to zero in between [107, 108].

Now the question arises what the relationship is between the initial state spin polarization effects described in this section and the final state as well as matrix element effects described in the previous sections. As stated before it can be expected that the photoelectrons are spin polarized if the spin–orbit splitting is resolved somewhere in the experiment. For the Rashba systems this happens in the initial state, if one were to integrate over a symmetric angle around normal emission it would not be possible to resolve the spin splitting. Because of the spin–momentum locking, Rashba systems and topological insulators have a well-defined spin quantization axis. Let us assume as a first approximation that in the Rashba system the initial states are pure s states which show a spin splitting in angle-resolved photoemission. The spin–orbit interaction does not influence the nature of the ground state angular momentum since the orbital angular momentum is zero there.

Changes of the spin polarization of the initial states due to the photoexcitation and the photoelectron emission process may arise due to the spin–orbit-induced effects in photoemission as discussed in the previous sections: chirality in the photoemission according to a one-step process including the influence of the crystal surface (section 6), phase shift effects as discussed in sections 3 and 4 and matrix element effects in photoemission by circularly polarized radiation (sections 1 and 2). For the Au(111) surface state it was, for example, predicted that the chiral target effects described in section 6 should be observable at normal emission [76]. Up to now this predicted out-of-plane polarization at normal emission has not been unambiguously observed. However, given the fact that most SARPES measurements on Rashba systems are performed on (111) surfaces of fcc crystals, this could be a general effect which needs to be taken into account for a detailed analysis of the

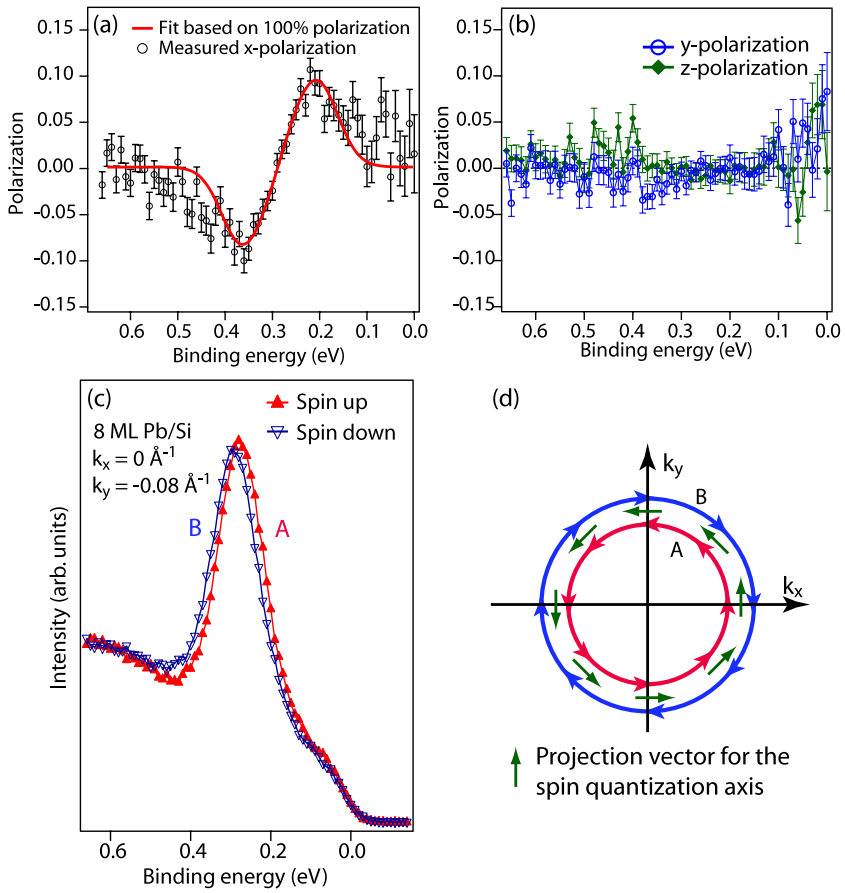

Figure 37. Spin- and angle-resolved photoelectron spectra for a 8 ML thick Pb layer on Si(111) $\sqrt{3}$. (a) Spin polarization in x-direction, (b) in y and z directions, (c) partial spin-resolved photoelectron spectra in x direction and (d) schematic diagram of a constant energy surface with arrows of the spin polarization direction [96]. From [96].

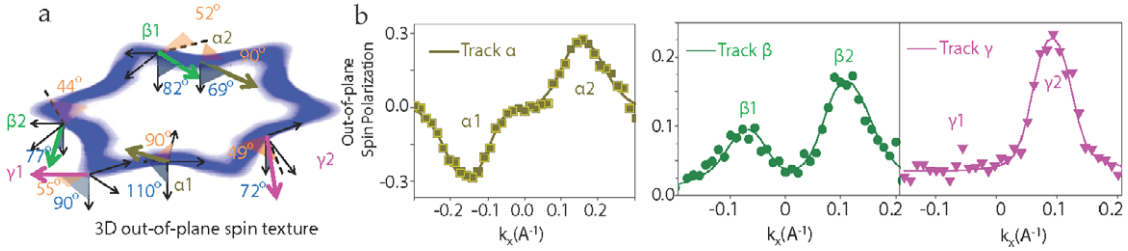

Figure 38. 3D spin structure of the topological insulator Bi_2Te_3 under the influence of warping. (a) Summary of the 3D spin polarization vectors on the snowflake Fermi surface for six measured band crossings $\alpha_{1,2}$, $\beta_{1,2}$ and $\gamma_{1,2}$ shown by out-of-plane angle (blue) and in-plane angle (orange). (b) Measured out-of-plane spin polarization (P_z) spectra of tracks α, β and γ, where the tracks are defined by a straight line between the respective points [108]. From [108].

spin structure and be separated from the initial state spin structure.

As has been shown in atomic photoionization, phase shift effects in the final states exist if two final states of different orbital angular momentum are occupied due to the selection rules for dipole transition $\Delta l = +1, -1$ and interfere in photoemission with each other with the consequence that the photoelectrons are highly spin polarized even if they are ejected by linearly polarized or even unpolarized radiation according to equations (2)–(4). This is not the case for photoionization starting from s-initial states.

A non-negligible phase shift between $p_{3/2}$ and $p_{1/2}$, $d_{5/2}$ and $d_{3/2}$, and $f_{7/2}$ and $f_{5/2}$ final states only due to an influence of the spin–orbit interaction there, has never been experimentally observed nor theoretically calculated outside resonance processes [109, 2] as also shown in figure 32. Thus phase shift effects (with the consequence that photoelectrons ejected by linearly polarized or unpolarized radiation are spin polarized) only exist if the initial states show a pronounced hybridization or have contribution of a non-vanishing orbital angular momentum and their spin–orbit-induced fine structure splitting is resolved in the photoelectron spectrum. Their dynamical spin polarization would be perpendicular to the reaction plane defined by the electric E vector and the Rashba spin orientation of the initial state and is proportional to $\sin^r\theta\cos^s\theta$ with θ being the angle between these two

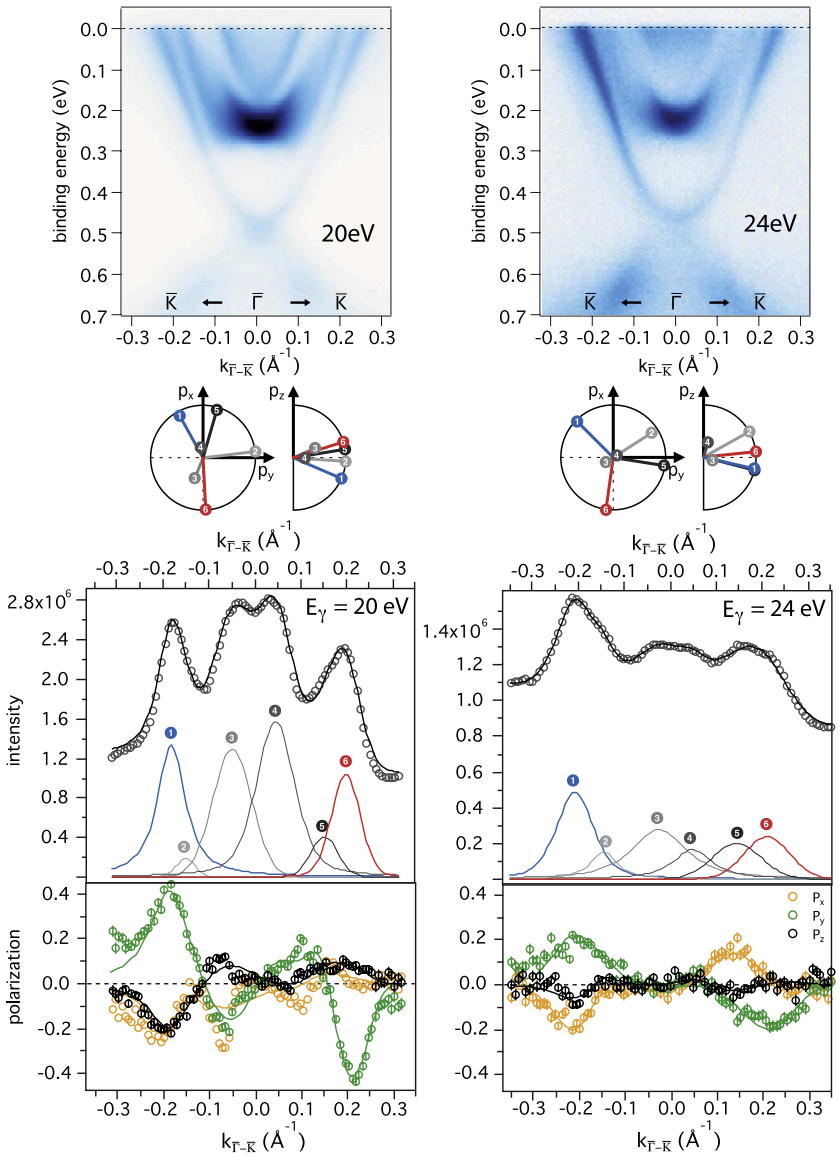

Figure 39. Comparison of the measured spin polarization for $PbBi_4Te_7$ at 20 eV (left) and 24 eV (right). From top to bottom the different panels show the measured spin integrated band map along ΓK, the spin polarization vectors obtained from the fit, the total measured intensity for an MDC at E_F and the simultaneously measured spin polarization along the three spatial components [110]. From [110].

directions and r and s being integer numbers from 1 up to $(2l+1)$ with l as orbital angular momentum of the initial state. Note that this dynamical spin polarization always vanishes at $\theta = 0°$ and 90°.

On the other hand, in crystals with inversion symmetry the bulk bands should show no Rashba-type spin–orbit splitting, meaning that for these states no spin quantization axis is defined by the initial state. As a result phase shift effects can play a significant role. In the top panels of figure 39 the spin integrated band structure of the topological insulator $PbBi_4Te_7$ is shown for two different photon energies (20 and 24 eV) [110]. Between a binding energy of 0.5 and 0.3 eV only the Dirac state is observed, while at lower binding energies additional bands show up at lower momentum values. Apart from a change in intensity there is no clear dispersion between these two photon energies. In the bottom panels of figure 39 we show the corresponding SARPES data measured as a momentum distribution curve at the Fermi energy. If we only consider the data obtained at 20 eV it appears as if the bands at lower momentum values are spin polarized, evident from the well-defined spin polarization vectors extracted from the data. After changing the photon energy to 24 eV the spin polarization vectors of the Dirac state do not change, whereas those of the inner bands show a strong photon energy dependence and appear to break time reversal symmetry at 24 eV. This is a clear indication that the polarization vector of the Dirac state is an initial state effect and that of the other bands a final state effect, allowing us to identify these bands as spin-degenerate bulk bands. That these bands do show up as spin polarized in the SARPES experiment is due to the phase shift effects described in section 4.

If circularly polarized radiation is used in photoemission or the target itself is chiral in the photoemission process, a spin polarization transfer due to matrix element effects (optical

pumping) takes place as discussed in sections 1 and 2; in all systems the Rashba spin polarization may thus significantly change its direction and value. This is also the case for pure initial s states, comparable to the original Fano effect with alkali atoms as presented in figure 1 and discussed in section 1.

Baum *et al* [111] have experimentally studied this effect with free alkali atoms being spin polarized in the ground state by use of a Stern–Gerlach hexapole magnet. Thus the spin polarization transfer can be easily calculated for this photoionization process from the spin polarized ground states as given in [3]. When the helicity of the radiation is parallel to the Rashba initial state spin, its existing complete spin polarization stays as it is since it cannot be increased by spin polarization transfer. However, if they are antiparallel, a spin flip takes place which strongly depends upon the photon energy and upon the photoelectron emission angle. For example, in figure 1 at 290 nm the 'wrong' spin completely flips by 180° for all emission angles. At 265 nm no spin flip takes place and the spin polarizations stay as they have been in the initial states. The quantity of the spin flip depends upon the ratio $\rho = R_3/R_1$ of the dipole radial matrix elements for transition of $s_{1/2} \rightarrow p_{3/2}$ and $s_{1/2} \rightarrow p_{1/2}$, respectively. It is given by the following equations for this case:

$$P_{\text{anti}} = \frac{2(\rho-1)^2|Y_{10}|^2 - (2\rho+1)^2|Y_{11}|^2}{2(\rho-1)^2|Y_{10}|^2 + (2\rho+1)^2|Y_{11}|^2} \quad (7)$$

$$P_{\text{anti}} = \frac{\cos^2\theta[4(\rho-1)^2 + (2\rho+1)^2] - (2\rho+1)^2}{\cos^2\theta[4(\rho-1)^2 - (2\rho+1)^2] + (2\rho+1)^2} \quad (8)$$

with Y_{lm} being the spherical harmonics with θ the photoelectron emission angle and P_{anti} the photoelectron spin polarization for antiparallel initial spin and helicity.

Equations (7) and (8) directly show: if $\rho = 1$ (as it was in figure 1 at 265 nm) $P_{\text{anti}} = -1$, i.e. no spin flip occurs. The same happens for all photon energies if $\theta = 90°$, i.e. for perpendicular emission which means emission normal to the crystal surface if the Rashba polarization is in plane. The spin flip is always complete, i.e. $P_{\text{anti}} = 1$, for $\theta = 0°$ for all photon energies. This would have the consequence for the Rashba effect in photoemission that, when the photoemission is angle-resolved studied with circularly polarized radiation parallel or antiparallel to the radiation helicity, a Rashba spin orientation would be conserved quantitatively if it is parallel to the light helicity and it would be completely turned by 180° if it is antiparallel.

In the ARPES community most experimentalists are familiar with intensity matrix element effects based on three contributions: the dipole transition, the availability of a final state and photoelectron diffraction. Although hard to predict *a priori* these matrix element effects are often used to determine band symmetries or to enhance the contrast in the spectral function. Analogously one can think of spin matrix element effects, where the photoemission process selects one spin direction rather than another. For localized states these can be predicted along the lines of section 4, while for the delocalized states close to the Fermi level which have become the recent focus of SARPES measurements, this prediction

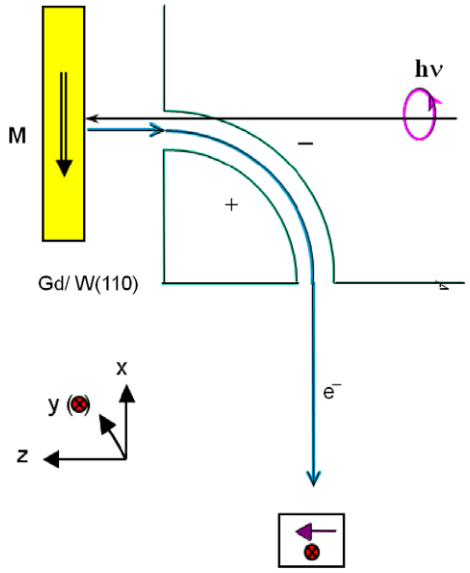

Figure 40. Scheme of the experiment by [113]. From [113].

is less obvious. However, as shown above these effects can be very useful in determining what part of the measured spin polarization is due to the spin polarized nature of the initial states, and which states are spin degenerate in the initial state. A systematic study for different photon energies should then also be able to disentangle the here-mentioned phase shift effects from spin polarization induced in the bulk bands by the finite probe depth of SARPES [112]. The first change rapidly with photon energy, whereas the latter should show only a very limited dependence.

Finally it should be mentioned that all effects superpose in three dimensions, if they jointly exist. A special case of coherent superposition is discussed in section 8.

8. Interference of spin states creating a rotation of the spin polarization vector

Whenever two states overlap in time and energy and they are not orthogonal to each other, they may interfere. If they are spin polarized with different directions of the spin polarization vector, a constructive interference of the spinors lets the spin rotate in space. This has been experimentally verified by Müller *et al* [113] according to the experimental set-up given in figure 40: the first spin polarization direction is the transferred spin polarization of the circularly polarized photons along z normal to the surface due to the spin–orbit interaction if this is resolved in the experiment. The second one is the exchange-interaction-induced spin polarization of an in-plane magnetized Gd(0001) film on W(110). The resonant photoemission process was performed by use of circularly polarized synchrotron radiation. With the optical selectivity of performing the photoabsorption at a certain wavelength, a $^8D_{9/2}$ intermediate spin–orbit fine structure state is excited which decays very quickly via a super-Coster–Kronig decay into the photoemission continuum. Since the $^8D_{9/2}$ resonance is spin–orbit-resolved and separated from other fine structure components, the

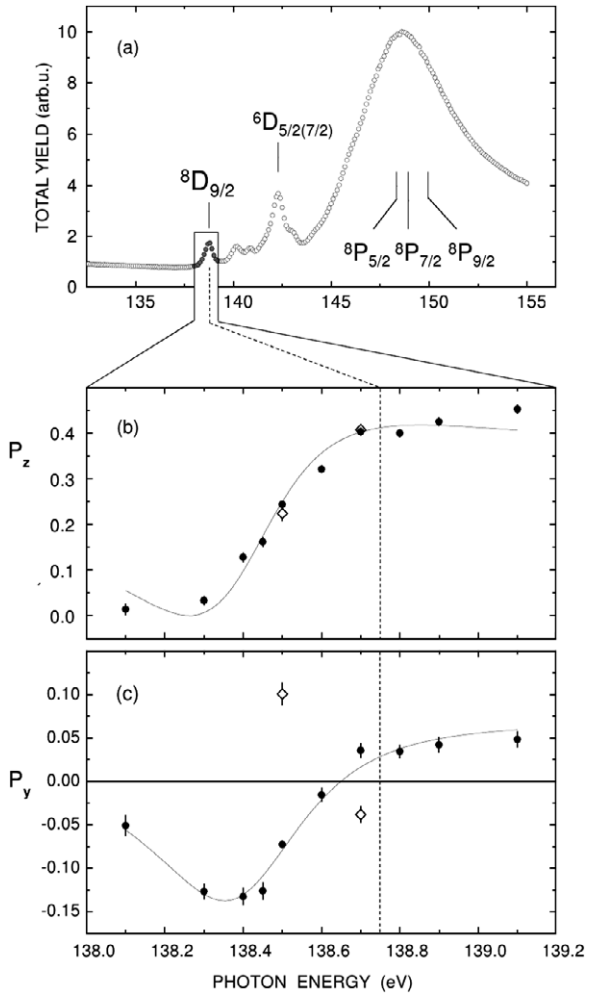

Figure 41. (a) Total yield spectrum of photoelectrons near the Gd 4d → 4f resonance (b) and (c) spin polarization components P_z and P_y measured across the first pre-edge peak at a photon energy of 138.75 eV. Open diamonds show the results obtained with reversed magnetization [113]. The corresponding experimental set-up is given in figure 40. From [113].

photoelectrons are spin polarized along the direction of the light helicity as described in section 2. But additionally a direct photoexcitation and emission may also take place from the in-plane spin polarized magnetic band states to the photoemission continuum, giving polarized photoelectrons parallel to the magnetization. When both spin directions, spin–orbit and exchange-induced, constructively interfere a third spin component perpendicular to both initials should exist. This has been experimentally verified [113] as shown in figure 41. A third component P_y perpendicular to P_z and to the magnetization in the x direction has been measured which switches its sign if the magnetization is reversed. Across the $^8D_{9/2}$ resonance of the resonant photoemission process this new spin polarization component changes its sign which is typical for constructive and destructive interferences within a Fano-type autoionization resonance [114, 20, 41].

A similar effect of interference of spin states has been recently reported by Meier *et al* [115] in photoemission from Sb/Ag(111). Using a three-dimensional spin polarization detector an intrinsic overlap of states with orthogonal spins of the Rashba-type splitting has been observed. They observed a large spin polarization in-plane component but normal to the quantization axis provided by the Rashba effect. Figure 42 shows the experimental results: the Rashba-induced spin polarizations of the opposite y direction, not resolved in the spin integrated experiment (see figures 42(b) and (c)), interfere with each other creating a rotated spin polarization in the x and z directions as given in figure 42(d) [115].

9. Cross-comparison of spin-resolved photoemission above the Curie temperature with magnetic circular dichroism asymmetry in intensity below the Curie temperature

It is well known that photoemission of magnetized, i.e. spin oriented, matter by use of circularly polarized radiation creates a magnetic circular dichroism (MCD) in the intensity of the photoelectrons emitted, i.e. the yield of photoelectrons is different if the light helicity and the initial spin orientation of the ferromagnet is parallel or antiparallel [116]. It is also a well-established technique to use this dichroic asymmetry of photoabsorption yield to experimentally determine the local magnetic momenta of the spin and orbit of the ferromagnetic system by use of sum rules.

Atomic theory in electric dipole approximation has shown that circular dichroism in photoabsorption of spin oriented atoms and its angular intensity distribution of photoelectrons emitted are directly correlated to the spin polarization of photoelectrons from unpolarized paramagnetic atoms excited by circularly polarized radiation [117]. In particular, in cases where phase shift effects as discussed in section 3 are excluded or do not play a role, for example in photoelectron emission directions of the so-called magic angle where $P_2(\cos\theta) = 0$ in equation (1), the MCD intensity asymmetry is quantitatively given by the spin polarization of the photoelectrons but with the opposite sign [117]. It thus makes no difference whether one starts the photoemission process with a spin oriented system and measures the photoelectron intensity asymmetry under switching the radiation helicity from left to right or one measures the photoelectron spin polarization after the photoemission process of an unpolarized system. This equality of physical information in both types of experiment is, of course, only valid if the exchange interaction splitting (m-substates) are not spectroscopically resolved in the MCD photoemission experiment, which is mostly the case.

Müller *et al* [24] experimentally demonstrated this for the first time in resonant 4d–4f photoemission of Gd and have proved that MCD investigations of a magnetically ordered system, measured by [116], and spin polarization measurements in a magnetically non-ordered state yield corresponding results. This is shown in figure 43 where both types of experiment yield the same experimental results for the total yield (upper part of figure 43) and the same values of the spin polarization and of the MCD asymmetry, apart from the different sign (lower part of figure 43). It is worth noting that the MCD experiment [116] with Gd(0001)/W(110) below

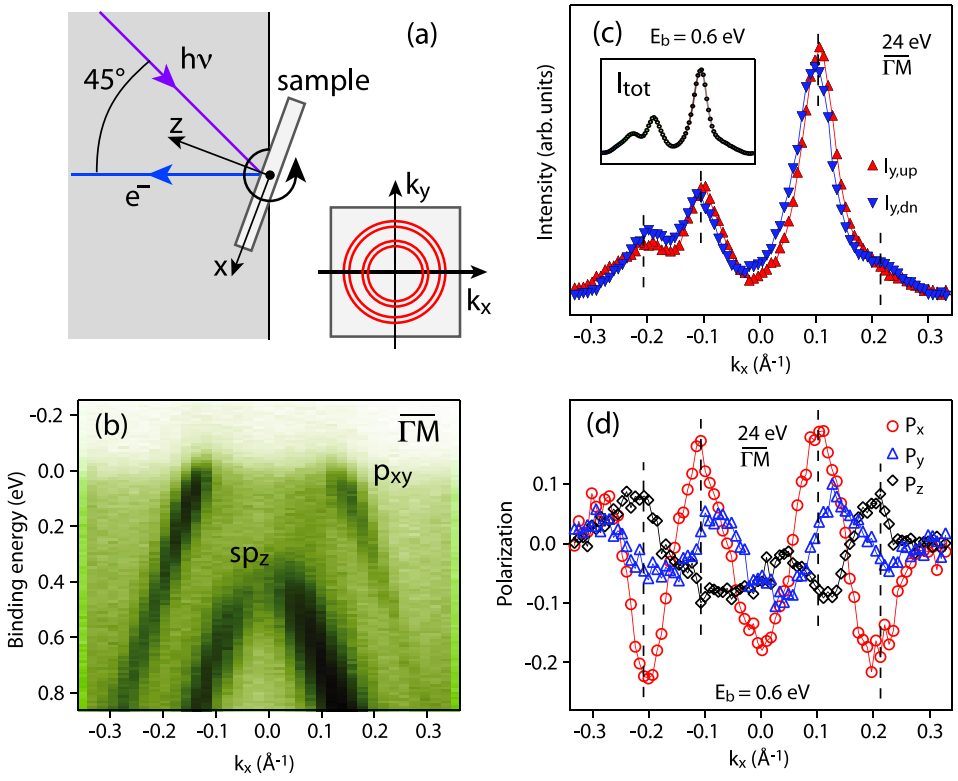

Figure 42. (a) Experimental set-up used in [115]. (b) Spin integrated surface band structure of Sb/Ag(111) [115]. (c) Spin-resolved and spin integrated (inset) partial intensities at a binding energy of 0.6 eV [115]. (d) The three simultaneously measured spin polarization components of photoemission of Sb/Ag(111). P_x and P_z are based upon the interference of the two Rashba split states oppositely polarized in y direction [115].

the Curie temperature was performed in grazing incidence of circularly polarized radiation because of the in-plane magnetization whereas the spin-resolved photoemission experiment [24] with Gd(0001)/W(110) above the Curie temperature used normal incidence of the circularly polarized radiation and normal emission of the photoelectrons detected. Thus spin-resolved photoemission data of a paramagnetic system can also be used to determine spin and orbital local magnetic moments like the use of MCD below the Curie temperature. This is, of course, an enormous experimental advantage if the Curie temperature is very low as for layers of molecular magnets. This was experimentally demonstrated very recently for adsorbed molecules with Mn^{II} as the main paramagnetic part in each one as shown in figure 44 [118]. The comparison of MCD asymmetry [119] to the results of spin-resolved electron spectroscopy [118] again shows that spin polarization measurements of magnetically non-ordered samples lead to results that are otherwise accessible via MCD/XAS intensity asymmetry measurements of samples magnetically oriented in strong magnetic fields (5 T) and at lowest temperatures (5 K).

10. Conclusions and outlook

The existence of polarized photoelectrons in angle-resolved photoemission of free atoms, molecules, adsorbates and condensed matter has been experimentally found to be the general case due to the existence and influence of the spin–orbit interaction. If its influence is somewhere experimentally resolved in the photoexcitation or photoemission experiment, for example by means of resolving the fine structure splitting of ground, intermediate or final state of the optical transition using a monochromator or an electron spectrometer, the photoelectrons are almost always highly spin polarized regardless of whether circularly polarized, linearly polarized or even unpolarized radiation is used. The spin polarization of the photoelectron may be induced by matrix element or by phase shift effects during the optical transition and during the path through the solid. Coherent or incoherent superpositions of different channels may strongly influence the results; chiral structures and aligned orientations of crystal surface structures also play important roles. However, the cross-comparison of spin polarization effects in photoionization of free atoms with that of solid crystals allows disentanglement of the different effects which may simultaneously happen in spin-resolved photoemission of condensed matter.

For delocalized states the field of spin- and angle-resolved photoemission is rapidly developing. It has been found that the phase shift and spin transfer effects also in this case cause the photoelectrons to be spin polarized if studied with high enough energy and angular resolution. When the spin–orbit interaction induces a spin polarization in the initial states (Rashba effect) primarily chiral effects are expected to play a role, but in this field there is still a need for further experiments to elucidate all possible spin effects. Finally it should be noted that the different spin–orbit

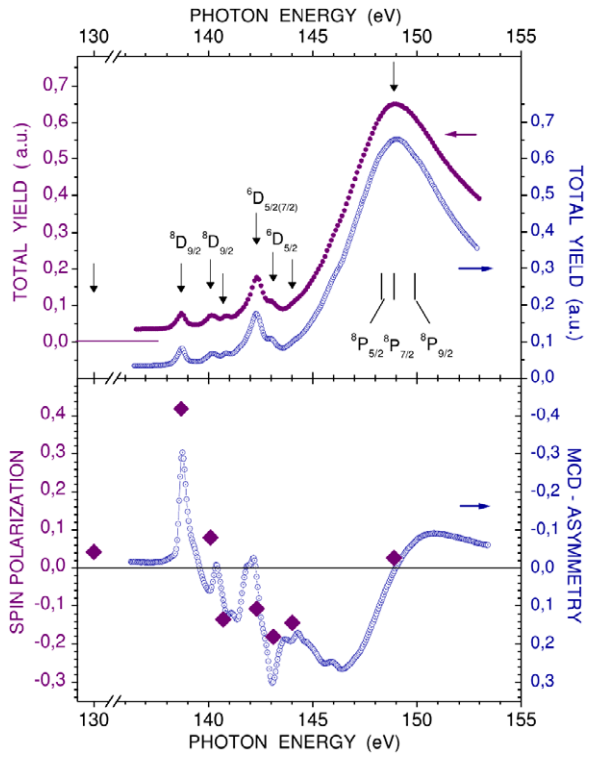

Figure 43. Upper panel (pink curve): x-ray absorption total yield spectrum measured at paramagnetic Gd(0001)/W(110) in the 4d–4f excitation region [24]. (Blue curve): corresponding total yield spectrum for ferromagnetic Gd(0001)/W(110) averaged for radiation of helicity parallel and antiparallel to the magnetization. The assignments of the resonances are given by and in accordance with [116, 24]. Lower panel: electron spin polarization *P* parallel to the radiation helicity (pink diamonds) measured at paramagnetic Gd(0001)/W(110) [24] in cross-comparison with the MCD asymmetry derived from [116, 24] for magnetized Gd below the Curie temperature (blue curve) referring to the right scale. Adapted from [116].

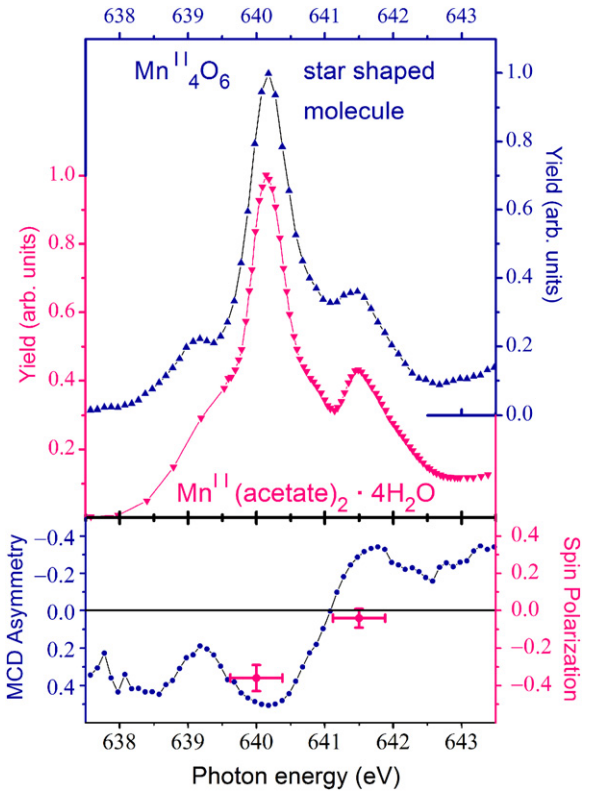

Figure 44. The analogous cross-comparison of MCD asymmetry for a magnetized Mn^{II} molecular target [118, 119] and photoelectron spin polarization from a Mn^{II} non-spin ordered paramagnetic molecular system [118] as in figure 43. MCD asymmetry (dotted) left axis, spin polarization (error crosses) right ordinate axis (lower part) in cross-comparison with the intensity yields obtained (upper part) [118].

interaction-induced spin polarization effects observed in photoemission of non-magnetic materials are also additionally present in photoemission of ferromagnetic targets, where a spin orientation due to exchange interaction is already present in the initial ground state. Its spin polarization is then changed in amount and direction during the photoemission process due to the additional influence of the spin–orbit interaction according to the rules discussed in this topical review. However, spin-resolved photoemission spectroscopy with non-magnetic materials and MCD intensity asymmetry studies with the analogous ferromagnetic target complement each other with respect to the goal of disentangling the influence of spin–orbit and exchange interaction as the two complementary mechanisms for electron spin orientation in matter.

Acknowledgments

UH gratefully acknowledges and deeply appreciates the very fruitful and successful scientific cooperation with N Müller during many joint experiments of spin-resolved photoemission over the past 27 years and the many scientific discussions with him to explain and to understand the new effects measured. Special thanks go to J Osterwalder and T Greber for intensive discussions on the joint research field of spin-resolved photoemission. Special thanks and regards also go to J Kessler of the University of Münster, for many discussions during the joint first 10 years of UH in spin-resolved photoelectron spectroscopy as well as during later visits, the last one in connection with his 80th birthday in 2010. JHD thanks G Bihlmayer for discussions concerning the theory of the Rashba effect. Technical support by A K Lofthouse and C Meier in preparing the manuscript is gratefully acknowledged. Financial, experimental and scientific support by the Universities of Karlsruhe, Münster and Bielefeld, the Fritz-Haber Institute of the MPG Berlin, BESSY (HZB), ELSA, ESRF, MaxLab and Swiss Light Source, the synchrotron radiation sources where the experiments have been performed, the BMBF, DFG and Swiss National Foundation is gratefully acknowledged.

References

[1] Fano U 1969 Spin orientation of photoelectrons ejected by circularly polarized light *Phys. Rev.* **178** 131–6
[2] Heinzmann U and Cherepkov N A 1996 VUV and soft x-ray photoionization studies *Spin polarization in photoionization* (*Physics of Atoms and Molecules*)

ed U Becker and D A Shirley (New York: Plenum) pp 521–59 and references therein
[3] Kessler J 1985 *Polarized Electrons* 2nd edn (Berlin: Springer)
[4] LaShell S, McDougall B A and Jensen E 1996 Spin splitting in an Au(111) surface state band observed with angle resolved photoelectron spectroscopy *Phys. Rev. Lett.* **77** 3419–22
[5] Fano U 1970 Spin–orbit coupling: a weak force with conspicuous effects *Comment. At. Mol. Phys.* **2** 30–6
[6] Heinzmann U 1980 Spin polarized photoelectrons from atoms and molecules *Appl. Opt.* **19** 4087–91
[7] Feder R 1985 *Polarized Electrons in Surface Physics* (Singapore: World Scientific)
[8] Kirschner J 1985 *Polarized Electrons At Surfaces* (Berlin: Springer)
[9] Heinzmann U 1987 Angle-, energy- and spin-resolved photoelectron emission using circularly polarized synchrotron radiation *Phys. Scr.* **T17** 77–88
[10] Heinzmann U 1990 Photoemission with circularly polarized photons *Photoemission and Absorption Spectroscopy of Solids and Interfaces with Synchrotron Radiation* ed M Campagna and R Rosei (Amsterdam: North-Holland) pp 469–88
[11] Heinzmann U and Schönhense G 1985 Spin-resolved photoemission from nonmagnetic metals and adsorbates *Polarized Electrons in Surface Physics* ed R Feder (Singapore: World Scientific) chapter 11, p 467
[12] Dil J H 2009 Spin- and angle resolved photoemission on non-magnetic low dimensional systems *J. Phys.: Condens. Matter* **21** 403001
[13] Heinzmann U, Kessler J and Lorenz J 1970 Wavelength dependence of the Fano effect *Phys. Rev. Lett.* **25** 1325
[14] Heinzmann U, Kessler J and Lorenz J 1970 Elektronen-Spinpolarisation bei der Photoionisation unpolarisierter Cäsiumatome mit zirkularpolarisiertem Licht *Z. Phys.* **240** 42
[15] Heinzmann U, Kessler J and Ohnemus B 1971 Polarized electrons by photoemission from solid alkalis *Phys. Rev. Lett.* **27** 1696
[16] Heinzmann U, Jost K, Kessler J and Ohnemus B 1972 Elektronen-Spinpolarisation beim Photoeffekt mit zirkularpolarisiertem Licht an Alkalischichten *Z. Phys.* **251** 354
[17] Pierce D T and Meier F 1976 Photoemission of spin polarized electrons from GaAs *Phys. Rev.* B **13** 5484
[18] Eyers A, Schäfers F, Schönhense G, Heinzmann U, Oepen H P, Hünlich K, Kirschner J and Borstel G 1984 Characterization of symmetry properties of Pt(111) electron bands by means of angle-, energy- and spin-resolved photoemission with circularly polarized synchroton radiation *Phys. Rev. Lett.* **52** 1559–62
[19] Snell G, Drescher M, Müller N, Heinzmann U, Hergenhahn U, Viefhaus J, Heiser F, Becker U and Brookes N B 1996 Spin polarized Auger electrons: the $XeM_{4,5}N_{4,5}N_{4,5}$ case *Phys. Rev. Lett.* **76** 3923
[20] Heinzmann U 1980 Experimental determination of the phase differences of continuum wavefunctions describing the photoionisation process of xenon atoms I. Measurements of the spin polarisations of photoelectrons and their comparison with theoretical results *J. Phys. B: At. Mol. Opt. Phys.* **13** 4353
[21] Heinzmann U 1977 An apparatus for the production of circularly polarised VUV radiation *J. Phys. E: Sci. Instrum.* **10** 1001
[22] Huth-Fehre T, Mank A, Drescher M, Böwering N and Heinzmann U 1990 Rotationally resolved Fano effect of HI molecules: an experimental study using coherent vacuum-ultraviolet radiation *Phys. Rev. Lett.* **64** 396
[23] Heinzmann U 1978 New vacuum ultraviolet absorption data for lead vapour obtained by spin polarisation measurements *J. Phys. B: At. Mol. Opt. Phys.* **11** 399
[24] Müller N, Lischke T, Weiss M R and Heinzmann U 2001 Spin resolved photoelectron spectroscopy from paramagnetic Gd at the 4d → 4f resonance using circularly-polarized radiation, a cross-comparison with MCD *J. Electron. Spectrosc.* **114–116** 777
[25] Wöhlecke M and Borstel G 1981 Group-theoretical study of light-induced electron-spin polarization at the Γ point of cubic crystals *Phys. Status Solidi* b **107** 653
[26] Cherepkov N A 1983 Spin polarization of atomic and molecular photoelectrons *Adv. Atom Mol. Phys.* **19** 395–447
[27] Thole B and van der Laan G 1991 Spin polarization and magnetic dichroism in photoemission from core and valence states in localized magnetic systems *Phys. Rev.* B **44** 12424
van der Laan G and Thole B 1993 Spin polarization and magnetic dichroism in photoemission from core and valence states in localized magnetic systems: emission from open shells II *Phys. Rev.* B **48** 210–23
Thole B and van der Laan G 1994 Spin polarization and magnetic dichroism in photoemission from core and valence states in localized magnetic systems: angular distributions III *Phys. Rev.* B **49** 9613–31
[28] Böwering N, Salzmann M, Müller M, Klausing H-W and Heinzmann U 1990 Photoelectron spin-polarization approaching unity: photoionization of Tl *Phys. Scr.* **41** 429–32
[29] Schönhense G, Eyers A, Friess U, Schäfers F and Heinzmann U 1985 Highly spinpolarized photoemission near threshold from physisorbed xenon and krypton atoms *Phys. Rev. Lett.* **54** 547–50
[30] Müller N, Kessler B, Schmiedeskamp B, Schönhense G and Heinzmann U 1987 Spin-resolved photoemission from Ir(111): transitions into a secondary band and energetic position of the final state bands *Solid State Commun.* **61** 187–92
[31] Noffke J and Fritsche L 1982 Band structure calculation and photoemission analysis of iridium *J. Phys. F: Met. Phys.* **12** 921–32
[32] Wöhlecke M and Borstel G 1984 *Optical Orientation, Modern Problems in Condensed Matter Sciences* vol 8, ed F Meier and B P Zakharchenya (Amsterdam: Elsevier) pp 423–3
[33] Drescher M, Snell G, Kleineberg U, Stock H-J, Müller N, Heinzmann U and Brookes N B 1997 Characterization of the helical undulator HELIOS I in the 520 to 930 eV range using a multilayer polarimeter *Rev. Sci. Instrum.* **68** 1939–44
[34] Khalil T, Schmidtke B, Drescher M, Müller N and Heinzmann U 2002 Experimental verification of quadrupole–dipole interference in spin-resolved photoionization *Phys. Rev. Lett.* **89** 053001
[35] Heinzmann U, Schönhense G and Wolcke A 1980 Spin polarized photoelectrons from unpolarized lead atoms exposed to unpolarized radiation *Proc. Int. Workshop on Coherence and Correlation in Atomic Collisions* ed H Kleinpoppen and J F Williams (New York: Plenum) pp 607–12
[36] Heinzmann U, Schönhense G and Kessler J 1979 Polarization of photoelectrons ejected by unpolarized light from xenon atoms *Phys. Rev. Lett.* **42** 1603–5

[37] Kaesdorf S, Schönhense G and Heinzmann U 1983 Angle- and spin resolved photoelectron spectroscopy on some halogen molecules *Ann. Isr. Phys. Soc.* **6** 179–81

[38] Schönhense G, Dzidzonou V, Kaesdorf S and Heinzmann U 1984 Spin polarized photoelectrons from randomly oriented halogen molecules by unpolarized radiation *Phys. Rev. Lett.* **52** 811–4

[39] Salzmann M, Böwering N, Klausing H W, Kuntze R and Heinzmann U 1994 Spin resolved photoelectron spectroscopy of HBr in the resonance region of electron autoionization *J. Phys. B: At. Mol. Opt. Phys.* **27** 1981–92

[40] Schönhense G 1980 Angular dependence of the polarization of photoelectrons ejected by plane-polarized radiation from argon and xenon atoms *Phys. Rev. Lett.* **44** 640–3

[41] Heinzmann U 1980 Experimental determination of the phase differences of continuum wavefunctions describing the photoionisation process at xenon atoms. II. Evaluation of the matrix elements and the phase differences and their comparison with data in the discrete spectral range in application of the multi channel quantum defect theory *J. Phys. B: At. Mol. Opt. Phys.* **13** 4367–81

[42] Cherepkov N A 1979 Spin polarization of photoelectrons ejected from unpolarised atoms *J. Phys. B: At. Mol. Opt. Phys.* **12** 1279–96

[43] Huang K N, Johnson W R and Cheng K T 1979 Theoretical study of spin polarisation of photoelectrons from noble gases *Phys. Rev. Lett.* **43** 1658–61

[44] Geiger J 1977 Energy loss spectra of xenon and krypton and their analysis by energy-dependent multichannel quantum defect theory *Z. Phys.* A **282** 129–41

[45] Schmidtke B, Drescher M, Cherepkov N A and Heinzmann U 2000 On the impossibility to perform a complete valence-shell photoionization experiment with closed-shell atoms *J. Phys. B: At. Mol. Opt. Phys.* **33** 2451–65

[46] Kessler B, Müller N, Schmiedeskamp B, Vogt B and Heinzmann U 1990 Spin resolved off-normal photoemission from xenon adsorbates in comparison with free atom photoionization *Z. Phys.* D **17** 11–6

[47] Stoppmanns P, David R, Müller N and Heinzmann U 1994 Angle and spin resolved Auger and photoelectron spectroscopy on Rb-layers by means of circularly polarized VUV radiation *Z. Phys.* D **30** 251–3

[48] Irmer N, David R, Schmiedeskamp B and Heinzmann U 1992 Experimental verification of a spin effect in photoemission: polarized electrons due to phase shift differences in the normal emission from Pt(100) by unpolarized radiation *Phys. Rev.* B **45** 3849

[49] Irmer N, Frentzen F, Schmiedeskamp B and Heinzmann U 1994 Spin polarized photoelectrons with unpolarized light in normal emission from Pt(110) *Surf. Sci.* **307–309** 1114

[50] Schmiedeskamp B, Irmer N, David R and Heinzmann U 1991 A new spin effect in photoemission with unpolarized light: experimental evidence of spin polarized electrons in normal emission from Pt(111) and Au(111) *Appl. Phys.* A **53** 418

[51] Rose H B, Fanelsa A, Kinoshita T, Roth Ch, Hillebrecht F U and Kisker E 1996 Spin–orbit-induced spin polarization in W4f photoemission *Phys. Rev.* B **53** 1630–4

[52] Yu S-W, David R, Irmer N, Schmiedeskamp B, Müller N, Heinzmann U and Cherepkov N A 1998 Determination of phase differences of transition matrix elements from Pt(110) by means of spin-resolved photoemission with circularly and linearly polarized radiation *Surf. Sci.* **416** 396–402

[53] Leschik G, Courths R, Wern H, Hüfner S, Eckardt H and Noffke J 1984 Band structure of platinum from angle resolved photoemission experiments *Solid State Commun.* **52** 221–5

[54] Noffke J 1995 private communication
Published in Irmer N, Frenzen F, David R, Stoppmanns P, Schmiedeskamp B and Heinzmann U 1995 Photon energy dependence of spin-resolved photoemission spectra in normal emission from Pt(110) by linearly polarized light *Surf. Sci.* **331** 1147

[55] Cavalieri A L *et al* 2007 Attosecond spectroscopy in condensed matter *Nature* **449** 1029–32

[56] Goulielmakis E *et al* 2004 Direct measurement of light waves *Science* **305** 1267

[57] Kazansky A K and Echenique P M 2009 One-electron model for the electronic response of metal surfaces to subfemtosecond photoexcitation *Phys. Rev. Lett.* **102** 177401

[58] Baggesen J C and Madsen L B 2008 Secondary electron cascade in attosecond photoelectron spectroscopy from metals *Phys. Rev.* A **78** 032903
Baggesen J C and Madsen L B 2009 Theory for time-resolved measurements of laser-induced electron emission from metal surfaces *Phys. Rev.* A **80** 030901

[59] Zhang C H and Thumm U 2009 Attosecond photoelectrons spectroscopy of metal surfaces *Phys. Rev. Lett.* **102** 123601

[60] Lemell C, Solleder B, Tökesi K and Burgdörfer J 2009 Simulation of attosecond streaking of electrons emitted from a tungsten surface *Phys. Rev.* A **79** 062901

[61] Zhang C H and Thumm U 2011 Streaking and Wigner time delays in photoemission from atoms and surfaces *Phys. Rev.* A **84** 033401

[62] Wigner E P 1955 Lower limit for the energy derivative of the scattering phase shift *Phys. Rev.* **98** 145

[63] Smith T F 1960 Lifetime matrix in collision theory *Phys. Rev.* **118** 349

[64] Schäfers F, Heckenkamp Ch, Müller M, Radojević V and Heinzmann U 1990 Hg 5d and 6s: multi-channel quantum-defect analysis of experimental data *Phys. Rev.* A **42** 2603

[65] Tamura E, Piepke W and Feder R 1987 New spin polarization effect in photemission from nonmagnetic surfaces *Phys. Rev. Lett.* **59** 934–7

[66] Schmiedeskamp B, Vogt B and Heinzmann U 1988 Experimental verification of a new spin-polarization effect in photoemission: polarized photoelectrons from Pt(111) with linearly polarized radiation in normal incidence and normal emission *Phys. Rev. Lett.* **60** 651–4

[67] Mayer S and Kessler J 1995 Experimental verification of electron optic dichroism *Phys. Rev. Lett.* **74** 4803–6

[68] Nolting C, Mayer S and Kessler J 1997 Electron dichroism—new data and an experimental cross-check *J. Phys. B: At. Mol. Opt. Phys.* **30** 5491–9

[69] Ray K, Ananthavel S P, Waldeck D H and Naaman R 1999 Asymmetric scattering of polarized electrons by organized organic films of chiral molecules *Science* **283** 814–6

[70] Böwering N, Lischke T, Schmidtke B, Müller N, Khalil T and Heinzmann U 2001 Asymmetry in photoelectron emission from chiral molecules induced by circularly polarized light *Phys. Rev. Lett.* **86** 1187

[71] Göhler B, Hamelbeck V, Markus T Z, Kettner M, Hanne G F, Vager Z, Naaman R and Zacharias H 2011 Spin selectivity in electron transmission through self-assembled monolayers of double stranded DNA *Science* **331** 894–7

[72] Dresselhaus G 1955 Spin–orbit coupling effects in zinc blende structures *Phys. Rev.* **100** 580

[73] Bychkov Y A and Rashba E I 1984 Oscillatory effects and the magnetic susceptibility of carriers in inversion layers *J. Phys. C: Solid State Phys.* **17** 6039–45

[74] Hoesch M, Muntwiler M, Petrov V N, Hengsberger M, Patthey L, Shi M, Falub M, Greber T and Osterwalder J 2004 Spin structure of the Shockley surface state on Au(111) *Phys. Rev.* B **69** 241401

[75] Muntwiler M, Hoesch M, Petrov V, Hengsberger M, Patthey L, Shi M, Falub M, Greber T and Osterwalder J 2004 Spin- and angle-resolved photoemission spectroscopy study of the Au(111) Shockley surface state *J. Electron Spectrosc. Relat. Phenom.* **137-140** 119–23

[76] Henk J, Hoesch M, Osterwalder J, Ernst A and Bruno P 2004 Spin–orbit coupling in the L gap surface states of Au(111): spin-resolved photoemission experiments and first principles calculations *J. Phys.: Condens. Matter* **16** 7581–97

[77] Koroteev Yu M, Bihlmayer G, Gayone J E, Chulkov E V, Blügel S, Echenique P M and Hofmann Ph 2004 Strong spin–orbit splitting on Bi surfaces *Phys. Rev. Lett.* **93** 046403

[78] Hirahara T *et al* 2007 Direct observation of spin splitting in bismuth surface states *Phys. Rev.* B **76** 153305

[79] Bihlmayer G, Koroteev Y M, Echenique P M, Chulkov E V and Blügel S 2006 The Rashba-effect at metallic surfaces *Surf. Sci.* **600** 3888–91

[80] Nagano M, Kodama A, Shishidou T and Oguchi T 2009 A first-principle study on the Rashba effect in surface systems *J. Phys.: Condens. Matter* **21** 064239

[81] Ast C R, Henk J, Ernst A, Moreschini L, Falub M C, Pacilé D, Bruno P, Kern K and Grioni M 2007 Giant spin splitting through surface alloying *Phys. Rev. Lett.* **98** 186807

[82] Meier F, Dil H, Lobo-Checa J, Patthey L and Osterwalder J 2008 Quantitative vectorial spin analysis in angle-resolved photoemission: Bi/Ag(111) and Pb/Ag(111) *Phys. Rev.* B **77** 165431

[83] Lobo-Checa J, Meier F, Dil J-H, Okuda T, Corso M, Petrov V N, Hengsberger M, Patthey L and Osterwalder J 2010 Robust spin polarization and spin textures on stepped Au(111) surfaces *Phys. Rev. Lett.* **104** 187602

[84] Crain J N, Kirakosian A, Altmann K N, Bromberger C, Erwin S C, McChesney J L, Lin J-L and Himpsel F J 2003 Fractional band filling in an atomic chain structure *Phys. Rev. Lett.* **90** 176805

[85] Okuda T *et al* 2010 Large out-of-plane spin polarization in a spin-splitting one-dimensional metallic surface state on Si(557)–Au *Phys. Rev.* B **82** 161410(R)

[86] Wells J W *et al* 2009 Nondegenerate metallic states on Bi(114): a one-dimensional topological metal *Phys. Rev. Lett.* **102** 096802

[87] Krupin O, Bihlmayer G, Starke K, Gorovikov S, Prieto J E, Dobrich K, Blügel S and Kaindl G 2005 Rashba effect at magnetic metal surfaces *Phys. Rev.* B **71** 201403

[88] Meier F 2010 *PhD Thesis* University of Zurich

[89] Bentmann H, Kuzumaki T, Bihlmayer G, Blügel S, Chulkov E V, Reinert F and Sakamoto K 2011 Spin orientation and sign of the Rashba splitting in Bi/Cu(111) *Phys. Rev.* B **84** 115426

[90] Budde K, Abram E, Yeh V and Tringides M C 2000 Uniform, self-organized, seven-step height Pb/Si(111)-(7 × 7) islands at low temperatures *Phys. Rev.* B **61** R10602

[91] Mans A, Dil J-H, Ettema A R H F and Weitering H H 2002 Quantum electronic stability and spectroscopy of ultrathin Pb films on Si(111)7 × 7 *Phys. Rev.* B **66** 195410

[92] Upton M H, Wei C M, Chou M Y, Miller T and Chiang T-C 2004 Thermal stability and electronic structure of atomically uniform Pb films on Si(111) *Phys. Rev. Lett.* **93** 026802

[93] Dil J H, Kim J W, Kampen Th, Horn K and Ettema A R H F 2006 Electron localization in metallic quantum wells: Pb versus In on Si(111) *Phys. Rev.* B **73** 161308

[94] Chiang T C 2000 Photoemission studies of quantum well states in thin films *Surf. Sci. Rep.* **39** 181–235

[95] Dil J-H, Kim J W, Gokhale S, Tallarida M and Horn K 2004 Self-organization of Pb thin films on Cu(111) induced by quantum size effects *Phys. Rev.* B **70** 045405

[96] Dil J H, Meier F, Lobo-Checa J, Pathey L, Bihlmayer G and Osterwalder J 2008 Rashba-type spin–orbit splitting of quantum well states in ultrathin Pb films *Phys. Rev. Lett.* **101** 266802

[97] Slomski B, Meier F, Osterwalder J and Dil J H 2011 Controlling the effective mass of quantum well states in Pb/Si(111) by interface engineering *Phys. Rev.* B **83** 035409

[98] Slomski B, Landolt G, Meier F, Patthey L, Bihlmayer G, Osterwalder J and Dil J H 2011 Manipulating the Rashba-type spin splitting and spin texture of Pb quantum well states *Phys. Rev.* B **84** 193406

[99] Hasan M Z and Kane C L 2010 Topological insulators *Rev. Mod. Phys.* **82** 3045–67

[100] Frantzeskakis E and Grioni M 2011 Anisotropy effects on Rashba and topological insulator spin-polarized surface states: a unified phenomenological description *Phys. Rev.* B **84** 155453

[101] Hsieh D, Qian D, Wray L, Xia Y, Hor Y S, Cava R J and Hasan M Z 2008 A tunable topological insulator in the spin helical Dirac transport regime *Nature* **452** 970–4

[102] Hsieh D *et al* 2009 Observation of unconventional quantum spin textures in topological insulators *Science* **323** 919–22

[103] Xia Y *et al* 2009 Observation of a large-gap topological-insulator class with a single Dirac cone on the surface *Nature Phys.* **5** 398

[104] Zhang H, Liu C-X, Qi X-L, Dai X, Fang Z and Zhang S-C 2009 Topological insulators in Bi_2Se_3, Bi_2Te_3 and Sb_2Te_3 with a single Dirac cone on the surface *Nature Phys.* **5** 438

[105] Hsieh D *et al* 2009 A tuneable topological insulator in the spin helical Dirac transport regime *Nature* **460** 1101

[106] Fu L 2009 Hexagonal warping effects in the surface states of the topological insulator Bi_2Te_3 *Phys. Rev. Lett.* **103** 266801

[107] Souma S, Kosaka K, Sato T, Komatsu M, Takayama A, Takahashi T, Kriener M, Segawa K and Ando Y 2011 Direct measurement of the out-of-plane spin texture in the Dirac-cone surface state of a topological insulator *Phys. Rev. Lett.* **106** 216803

[108] Xu S Y *et al* 2011 Realization of an isolated Dirac node and strongly modulated spin texture in the topological insulator Bi_2Te_3, arXiv:1101.3985

[109] Fano U 1969 Spin orientation of photoelectrons: erratum and addendum *Phys. Rev.* **184** 250

[110] Eremeev S V *et al* 2012 Atom-specific spin mapping and buried topological states in a homologous series of topological insulators *Nature Commun.* **3** 635

[111] Baum G, Lubell M S and Raith W 1972 Measurement of the spin–orbit perturbation in the P-state continuum of heavy alkali-metal atoms: K, Rb and Cs *Phys. Rev.* A **5** 1073

[112] Kimura A *et al* 2010 Strong Rashba-type spin polarization of the photocurrent from bulk continuum states: experiment and theory for Bi(111) *Phys. Rev. Lett.* **105** 076804

[113] Müller N *et al* 2006 Interference of spin states in resonant photoemission induced by circularly polarized light from magnetized Gd *Phys. Rev.* B **74** 161401
[114] Heinzmann U, Heuer H and Kessler J 1975 Spin-polarized electrons from autoionizing transitions in thallium *Phys. Rev. Lett.* **34** 441–4
[115] Meier F, Petrov V, Mirhosseini H, Patthey L, Henk J, Osterwalder J and Dil J H 2011 Interference of spin states in photoemission from Sb/Ag(111) surface alloys *J. Phys.: Condens. Matter* **23** 072207
[116] Starke K, Navas E, Arenholz E, Hu Z, Baumgarten L, van der Laan G, Chen C T and Kaindl G 1997 Magnetic circular dichroism in 4d → 4f resonant photoemission and photoabsorption of Gd metal *Phys. Rev.* B **55** 2672–5
[117] Cherepkov N A and Kuznetsov V V 1989 Optical activity of polarised atoms *J. Phys. B: At. Mol. Opt. Phys.* **22** L405
[118] Helmstedt A *et al* 2011 Spin-resolved photoelectron spectroscopy of $[Mn_6^{III}Cr^{III}]^{3+}$ single-molecule-magnets and of manganese compounds as reference layers *J. Phys.: Condens. Matter* **23** 266001
[119] Khanra S *et al* 2008 Star-shaped molecule of MnO core with an S = 10 high-spin state. A theoretical and experimental study with XPS, XMCD and other magnetic methods *Inorg. Chem.* **47** 4605–17